THE MICROSTRUCTURE AND MATERIAL PROPERTIES OF THE EPICENTRAL TENDON-VERTEBRA ATTACHMENT IN RAINBOW TROUT

Emily MacMaster

Thesis submitted to the University of Ottawa
in partial fulfillment of the requirements for the
Master's degree in Biology

Department of Biology
Faculty of Science
University of Ottawa

ABSTRACT

Studies of the microstructure of tendon-bone attachments in mammals have shed light on their role in mediating efficient force transfer between tendon and bone, two tissues that differ vastly in their structure, composition, and material properties. Studies have also elucidated the importance of mechanical stimulation in maintaining tendon-bone attachment structures so that they may function successfully in dissipating mechanical stresses at the tendon-bone interface, to minimize the risk of tissue failure. Gross anatomical studies in fish have focused on identifying pathways of myomere contractile force transmission to the backbone of the fish, via connective tissue septa, to achieve body undulation. Little focus has been placed on how these connective tissues connect to the bone at the microscopic level to achieve force transfer. Moreover, whether or not these attachments are capable of undergoing remodeling in response to novel force regimes—which may influence their function—remains to be elucidated. First, we characterized the microstructure and material properties of the epicentral tendon-vertebra attachment in rainbow trout by conducting histology and tensile-testing. Individual collagen fibers of the epicentral tendon projected directly into the cancellous bone of the vertebra. We observed rostral-to-caudal trends in material properties for attachments found at different positions within the region spanning the dorsal and adipose fin, suggesting that attachments differed in their structure and/or composition at different positions along the backbone. Furthermore, the angle of the epicentral tendon with respect to the bone influenced the material properties and structural integrity of the attachments during tensile-testing, suggesting that attachments may be optimized to transfer force along particular angles. Second, we studied the effect of unloading on the material properties of the epicentral tendon-vertebra attachment by severing a subset of epicentral tendons on one side of rainbow trout. Severing of epicentral tendons had no effect on attachment material properties, suggesting that attachments did not undergo any alterations in structure and/or composition. We propose that the contiguous network of connective tissues in which the epicentral tendons are embedded as well as the fish's gross musculature may have supported the maintenance of function of the epicentral tendon-vertebra attachments.

ACKNOWLEDGEMENTS

I would like to thank my supervisors, Dr. Emily Standen and Dr. Odette Laneuville for allowing me to pursue a fourth-year honors project and Master's degree in their labs. Thank you both for your patience, guidance, and for giving me the flexibility to take the research in the directions that I wanted.

Keegan, Trina, Cassandra, Haodong, and Katherine for their endless help and support throughout this project.

The ACVS for the rearing of all fish used in experiments and for all their help and expertize when fish were recovering from surgery.

The technicians at the core histology facility and Clare Booth for all of their advice regarding the histological preparation of specimens.

My friends and family for all of their support and encouragement.

All fish used in the experiments underwent surgery and were euthanized according to University of Ottawa ACVS protocol BL-1926.

TABLE OF CONTENTS

LIST OF FIGURES

LIST OF TABLES

LIST OF ABBREVIATIONS

ANOVA	Analysis of Variance
APR	Anterior-Posterior Region
den DF	Denominator Degrees of Freedom
ENT	Epineural Tendon
EPT	Epipleural Tendon
Fig.	Figure
H&E	Hematoxylin and Eosin
HS	Horizontal Septum
LOESS	Locally Estimated Scatterplot Smoothing
LT	Lateral Tendon
MLR	Medio-Lateral Region
MS-222	Tricaine Methanesulfonate
MT	Myorhabdoid Tendon
num DF	Numerator Degrees of Freedom
POT	Posterior Oblique Tendon
R1-6	Regions 1-6
SE	Standard Error
TBL	Total Body Length
VS	Vertical Septum

CHAPTER 1.

Introduction

1.1 | INTRODUCTION

Within fish, a contiguous network of connective tissue septa (vertical septum, horizontal septum, myosepta) is proposed to be responsible for the transfer of myomere contractile forces to the backbone of the fish, causing bending and whole-body undulation. While a lot of gross anatomical work has been conducted in fish to identify pathways of force transmission via the connective tissue septa to the backbone, little is known about how these connective tissues connect with the backbone at the microscopic level to achieve force transfer. Furthermore, whether or not tendon-bone attachments in fish are capable of undergoing remodeling in response to mechanical stimulation, or lack thereof, has yet to be elucidated. The purpose of this study is to shed light on the microstructure and material properties of the epicentral tendon-vertebra attachment in rainbow trout, as well as study its ability to undergo remodeling in novel force regimes.

Components of the Vertebrate Musculoskeletal System

The primary roles of the vertebrate musculoskeletal system are to maintain the body's form and enable its movement. It is comprised of skeletal muscles and a diverse array of connective tissues, namely bones, cartilage, ligaments, and tendons. Connective tissues play an important role in the functioning of the musculoskeletal system: bones of the axial (skull, vertebral column, thoracic cage) and appendicular (pelvic and pectoral girdles, upper and lower limbs/fins) skeletons provide structural support and allow for movement; articular cartilage found at bone articulations minimizes friction between articulating bones; ligaments connect articulating bones and provide stability to the articulation; tendons connect muscles to bones, and transfer contractile forces generated by the skeletal muscles, to the bones of the skeleton, often to generate movement. Although skeletal muscle is capable of connecting to the bone directly (fleshy attachments), tendinous attachments are far more prominent within the human musculoskeletal system (Marieb & Hoehn, 2013) and likely all vertebrates.

Tendon-Bone Interfaces

Both tendon and bone consist primarily of extracellular matrix (water, fibrous proteins, proteoglycans, glycoproteins), with few cells embedded throughout. The structure and

composition of the extracellular matrix are what determine the material properties of tendon and bone. Tendon extracellular matrix is primarily composed of water and parallel arrays of collagen fibers (primarily type I) (Thorpe & Screen, 2016; Vogel & Koob, 1989). Other components include elastin, proteoglycans, and glycoproteins (Thorpe & Screen, 2016). Collagen provides the tendon with tensile strength, whereas elastin provides elasticity (Thorpe & Screen, 2016). Bone's primary extracellular matrix components are minerals (namely bioapatite), collagen (primarily type I), and water (Young, 2003). Bone mineral density is positively correlated with bone stiffness (Currey, 2011).

Specialized cells embedded within tendon and bone can contribute to the material properties and performance of these tissues, as they are responsible for maintaining and altering their extracellular matrix structure and composition. In vertebrate tendon, tenocytes and tenoblasts are responsible for secreting precursors of extracellular matrix components. Tenocytes are mature tenoblasts possessing an elongate morphology and a lower metabolic activity (Buschmann & Meier Bürgisser, 2017; Sai Chuen et al., 2004). Tenoblasts are characterised as being more rounded and as having a higher metabolic activity than tenocytes (Buschmann & Meier Bürgisser, 2017; Sai Chuen et al., 2004). Tenocytes have been reported to be evenly spaced, whereas tenoblasts have been reported to occur in clusters (Sai Chuen et al., 2004). Osteocytes, osteoblasts, and osteoclasts are three cell types found within and around vertebrate bone. It has been generally accepted that osteocytes are mechanosensing cells responsible for coordinating load-induced bone modeling and remodeling processes by signaling osteoblasts (bone-secreting cells found on bone surfaces) and osteoclasts (bone-resorbing cells found on bone surfaces) (J.-H. Chen, Liu, You, & Simmons, 2010; Nakashima et al., 2011). Osteocytes correspond to osteoblasts that have become embedded within the bone matrix that they secrete, culminating in their differentiation into osteocytes. They reside within lacunae, or small cavities, within the bone (Dean & Shahar, 2012; Noble, 2008).

Proper functioning of the vertebrate musculoskeletal system requires that forces produced by contracting muscles pass through tendon, to bone, via a typically tendinous interface (Fig. 1.1). The transfer of force across tissue interfaces where the interacting tissues differ in their structure, composition and therefore material properties, such as stiffness, poses challenges. Load-bearing structures are weakest where discontinuities in structure or composition cause mechanical stresses to concentrate, increasing the risk of structural failure (Pilkey, Pilkey, & Bi,

2020). Tendon and bone have very different structures, compositions, and stiffnesses (tendons are much less stiff than bone, mammalian elastic moduli are ~0.45GPa and ~20GPa, respectively) (Genin et al., 2009; Rossetti et al., 2017). As a result, the smooth flow of force from tendon to bone is interrupted at the interface of these two materials, generating stress concentrations at the interface, increasing the risk of attachment failure (Benjamin et al., 2002; Genin et al., 2009; Liu, Thomopoulos, Birman, Li, & Genin, 2012; Rossetti et al., 2017; Thomopoulos & Genin, 2013).

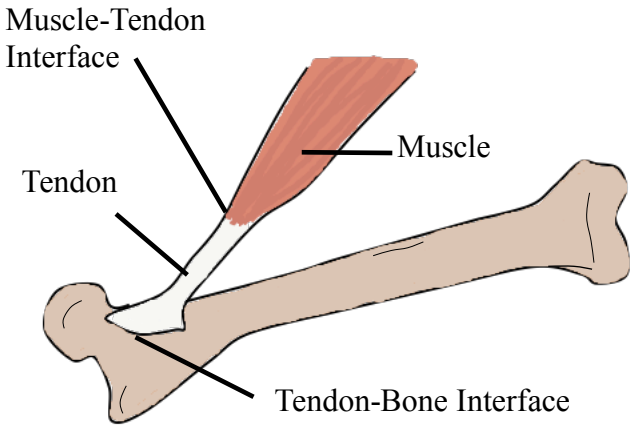

Fig. 1.1. Skeletal muscle attachment to bone, via tendon. Muscle-tendon and tendon-bone interfaces are indicated. Image has been modified from Anderson (2019).

The Responses of Tendon and Bone to Mechanical Stimulation or Lack Thereof

The specialized cells embedded within tendon and bone are capable of responding to mechanical stimulation, or lack thereof, by changing their densities and metabolic activities (often accompanied by changes in cell shape). In this way, they are capable of altering the extracellular matrix structure, composition, and material properties of these tissues. In vertebrate bone, mechanical stimulation has been shown to result in increased osteocyte density (Totland et al., 2011), increased bone formation (Atkins, Milgram, Weiner, & Shahar, 2015; Best, Holt, Troy, & Hamill, 2017; Sugiyama, Price, & Lanyon, 2010), increased bone mineral density (and stiffness) (Best et al., 2017; Fritton, Myers, Wright, & Van Der Meulen, 2005; Totland et al.,

2011), and changes in bone morphology (Du & Standen, 2020). Unloading of vertebrate bone has been shown to result in the apoptosis of osteocytes (Aguirre et al., 2006), decreased bone mineral density (and stiffness), increased bone resorption, and decreased bone strength (Friedman, Zhang, Wayne, Farber, & Donahue, 2019; Lang et al., 2004; Leblanc et al., 2000). In the tendon of vertebrates, mechanical stimulation has been shown to result in increased tenocyte density (Andersson et al., 2011), tenocyte rounding (Chicurel, Chen, & Ingber, 1998; Huisman, Lu, Mccormack, & Scott, 2014), and increased tenocyte metabolic activity (Huisman et al., 2014). Tenocytes with increased metabolic activity secrete extracellular matrix collagen precursors at a faster rate, which is linked to improved material properties of the tendon (Heinemeier & Kjaer, 2011). Vertebrate tendon has also been shown to respond to mechanical stimulation by increasing its diameter (linked to increased strength and stiffness) (Magnusson & Kjaer, 2003, 2019) and by becoming stiffer (Arampatzis, Peper, Bierbaum, & Albracht, 2010; Magnusson & Kjaer, 2019). Tendons subjected to compressive loads have been reported to develop a "crimp" morphology (Herchenhan et al., 2012), as well as fibrocartilage "pads" (Vogel & Koob, 1989) within regions of compression. Tendon crimp has been suggested to act as a shock absorber (Franchi et al., 2007) and therefore may aid in the dissipation of compressive stresses. The presence of fibrocartilage within the tendon at tendon-bone attachment sites has been proposed to facilitate a gradual bending of tendon collagen fibers and prevent slimming of the tendon at tendon-bone attachment sites (Benjamin & Ralphs, 1998). Unloading of vertebrate tendon has been shown to result in morphological changes, namely the misalignment of collagen fibers (Bayer, Schjerling, Herchenhan, Zeltz, & Heinemeier, 2014), the presence of tenocytes with a rounded morphology (Bayer et al., 2014), and decreased tendon cross-sectional area in cases where the tendon has experienced unloading for a prolonged period of time (Maganaris et al., 2006). Unloading of developing zebrafish tendons has also been shown to result in decreased length of tenocyte projections and decreased tendon extracellular matrix production. These effects were reversed by subjecting the developing tendons to loading (Subramanian, Kanzaki, Galloway, & Schilling, 2018).

Although most studies of bones and tendons have been conducted in mammals, we can also use the mammalian literature to generate hypotheses about fish. This is because fish bones and tendons share numerous features with those of mammals, including similar cell types (Bricard, Lebret, Lefevre, & Rescan, 2014; Witten & Huysseune, 2009), extracellular matrix compositions

(J. W. Chen et al., 2014; D. D. Lee & Glimcherl, 1991; Summers & Koob, 2002; Summers & Long, 2005), material properties (Summers & Koob, 2002; Summers & Long, 2005), and remodeling processes (Atkins et al., 2015; Subramanian et al., 2018; Totland et al., 2011). However, some morphological distinctions do exist between tendon and bone of fish and mammals, such as the hierarchal organization of tendon and bone in mammals (Summers & Koob, 2002; Summers & Long, 2005) and the tendinous sheet system in fish (Summers & Koob, 2002).

The Microscopic Structure of Tendon-Bone Attachments in Vertebrates

Types Identified by General Structure

Two main types of tendon-bone attachments have been identified and characterized in vertebrates at the microscopic level: *fibrocartilaginous* and *fibrous* (Fig. 1.2) (Benjamin et al., 2002; Hieronymus, 2006; Sanchez et al., 2013; Suzuki, Murakami, & Minoura, 2002, 2003). Fibrocartilaginous tendon-bone attachments are comprised of four zones: 1) tendon proper; 2) unmineralized fibrocartilage; 3) mineralized fibrocartilage; and 4) bone. Fibrous attachments consist of dense fibrous connective tissue and lack fibrocartilage. Two subtypes of fibrous attachments exist: *direct* and *indirect.* In the case of the former, tendon collagen fibers project directly into the bone; in the case of the latter, tendon fibers insert into the periosteum, which is connected to the bone. The periosteum consists of a connective tissue membrane that surrounds bones. It is comprised of two layers: an outer fibrous layer that is rich in collagen fibers, nerves, and blood vessels, and an inner cellular layer that is rich in osteoblasts. The periosteum is involved in bone growth and repair processes (Dwek, 2010; The Editors of Encyclopaedia Britannica, 2018). Variations of fibrocartilaginous attachments have also been identified and described at the microscopic level within lizards and crocodiles: variations in the amount of fibrocartilage present; differing degrees of distinction between the four zones; the presence of hyaline cartilage; the presence of a periosteum (Suzuki et al., 2002, 2003). An additional morphological feature of tendon-bone attachments are Sharpey's fibers (Benjamin et al., 2002; Hieronymus, 2006; Pereyra, Bona, Cerda, & Desántolo, 2019; Sanchez et al., 2013; Suzuki et al., 2002, 2003). These have been described in the literature as 'perforating fibers' that serve as anchors for tendons, ligaments, and periosteum connected to bone (Benjamin et al., 2002). The term 'Sharpey's Fibers' has been used to describe both the mineralized collagen fibers found

within the mineralized fibrocartilage zone of fibrocartilaginous tendon-bone attachments, as well as the perforating fibers found within the bone of fibrous attachments (Fig. 1.2).

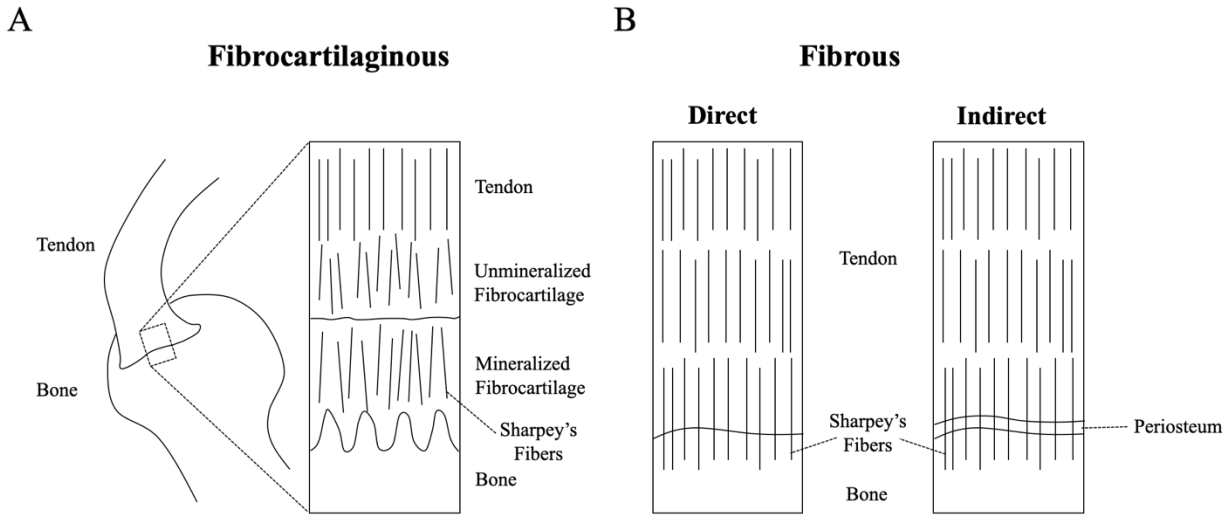

Fig. 1.2. Types of tendon-bone attachments and their basic microstructures. **A**, The microstructure of a fibrocartilaginous tendon-bone attachment. Vertical lines indicate collagen fibers. Collagen fibers have been shown to unravel, splay, and become increasingly misaligned within the zones of unmineralized and mineralized fibrocartilage (Genin et al., 2009; Rossetti et al., 2017). Schematic modified from Deymier-Black, Pasteris, Genin, & Thomopoulos (2015). **B**, The microstructures of direct and indirect fibrous tendon-bone attachments. Vertical lines indicate collagen fibers. Collagen fiber alignment has not been quantified within fibrous attachments.

Fibrocartilaginous tendon-bone attachments are described in the mammalian literature as playing an important role in the dissipation of mechanical stresses at the junction between tendon and bone. Several features contributing to force dispersion include gradual increased mineralization and decreased collagen fiber alignment in the direction of tendon to bone (Genin et al., 2009; Rossetti et al., 2017), the high concentration of negatively charged proteoglycans within the zones of unmineralized and mineralized fibrocartilage (Benjamin & Ralphs, 1998; Rossetti et al., 2017; Vogel & Koob, 1989), and a widened tendon footprint (Benjamin & Ralphs,

1998). Less is known about fibrous attachments outside of their general structure, as they are less common within mammals (Apostolakos et al., 2014).

Location

Fibrocartilaginous attachments are commonly found on the ends of long bones, termed epiphyses, in regions proximal to joints. Fibrous attachments are commonly found on the shafts of long bones, termed diaphyses, in regions distal to joints (Apostolakos et al., 2014). As previously mentioned, it has been proposed that the presence of fibrocartilage within tendon is an adaptation to compressive load (Benjamin & Ralphs, 1998; Vogel & Koob, 1989). As fibrocartilaginous attachments are found at the epiphyses of long bones in proximity to joints, their respective tendons experience greater changes in angle across a joint's range of motion compared to a tendon with a fibrous attachment. Consequently, fibrocartilaginous attachments experience a greater degree of compressive load than fibrous attachments (Benjamin & Ralphs, 1998). As a result, Benjamin & Ralphs (1998) argue that the presence or absence of fibrocartilage at the interface between tendon and bone is related to the angle change (and extent of compressive load) that the respective tendon experiences relative to the bone, during force transmission (Benjamin & Ralphs, 1998).

The Response of Tendon-Bone Attachments to Mechanical Stimulation

Tendon and bone attachments undergo structural and compositional remodeling when exposed to novel force regimes (Deymier et al., 2019; Gilotra, Shorofsky, Stein, & Murthi, 2016; Schwartz, Lipner, Pasteris, Genin, & Thomopoulos, 2013). Normal development and injury repair of fibrocartilage attachment sites require mechanical loading (Gilotra et al., 2016; Schwartz et al., 2013). Unloaded attachments show a decrease in collagen fiber alignment (Schwartz et al., 2013) and bone loss (Deymier et al., 2019), which could impact tissue function (Deymier et al., 2019). Sharpey's fibers also appear to remodel with changing force environments, but with variable responses (increased density and diameter in response to increased mechanical loading [J. E. Anderson, Lentz', Johnson, & Anderson, 1993; Barton & Keenan, 1967], increased fiber diameter in response to decreased loading [Short & Johnson, 1990], and no change in fiber morphology or density in response to loading [Turcotte, Green, Kupczik, McFarlin, & Schulz-Kornas, 2020]). In reptiles, muscle architecture—a proxy for the

extent of mechanical loading on bone—was positively correlated with Sharpey's fiber density, but shared no relationship with fiber diameter (Hieronymus, 2006).

The Fish Musculoskeletal System

Components

Fish have a complex musculoskeletal system composed of muscle segments (myomeres) nested within one another on either side of the fish's backbone (Fig. 1.3A) (Alexander, 1969). Two main types of muscle have been identified in most fish: white and red. Red muscle can be located internally, or laterally, as is the case in most species of fish, such as mackerel and rainbow trout (Fig. 1.3A) (Altringham & Ellerby, 1999; Syme & Shadwick, 2011). A contiguous network of connective tissues (skin, septa [vertical septum, myosepta, horizontal septum]) envelopes the myomeres (S. Gemballa, Hagen, Röder, Rolf, & Treiber, 2003; Westneat, Hoese, Pell, & Wainwright, 1993; Westneat & Wainwright, 2001). The skin forms the protective outer covering that contains all parts of the musculoskeletal system and has attachments to all myomeres and all septa. The vertical septum is a connective tissue sheet that separates the right and left sides of a fish's body and that binds together the neural and hemal spines of all vertebrae (Fig. 1.3B, C) (Westneat & Wainwright, 2001). The myosepta are connective tissue sheets that envelope and separate adjacent myomeres (Fig. 1.3A) (Sven Gemballa & Vogel, 2002). Six myoseptal tendons embedded within each myoseptum have been identified in jawed fish: epineural tendon (x1), epipleural tendon (x1), lateral tendons (x2), myrorhabdoid tendons (x2) (Fig. 1.3A) (Sven Gemballa et al., 2003; Sven Gemballa & Vogel, 2002). The horizontal septum is a connective tissue sheet that connects the vertebral column to the skin and separates the dorsal epaxial muscles from the ventral hypaxial muscles (Fig. 1.3) (S. Gemballa et al., 2003; Westneat et al., 1993; Westneat & Wainwright, 2001). In most species of fish, collagen fibers are embedded within the horizontal septum. These fibers can form distinct tendon-like bundles and run in opposite directions (*epicentral tendons* or *epicentral fibers* running caudolaterally; *posterior oblique tendons* or *posterior oblique fibers* running craniolaterally) (S. Gemballa et al., 2003; Westneat et al., 1993; Westneat & Wainwright, 2001). For instance, the horizontal septum of mackerel contains epicentral tendons and posterior oblique tendons (Fig. 1.3C) (Westneat et al., 1993; Westneat & Wainwright, 2001). Westneat et al. (1993, 2001) noted that, in mackerel, the angle of the epicentral tendon relative to the backbone increases towards the posterior of the

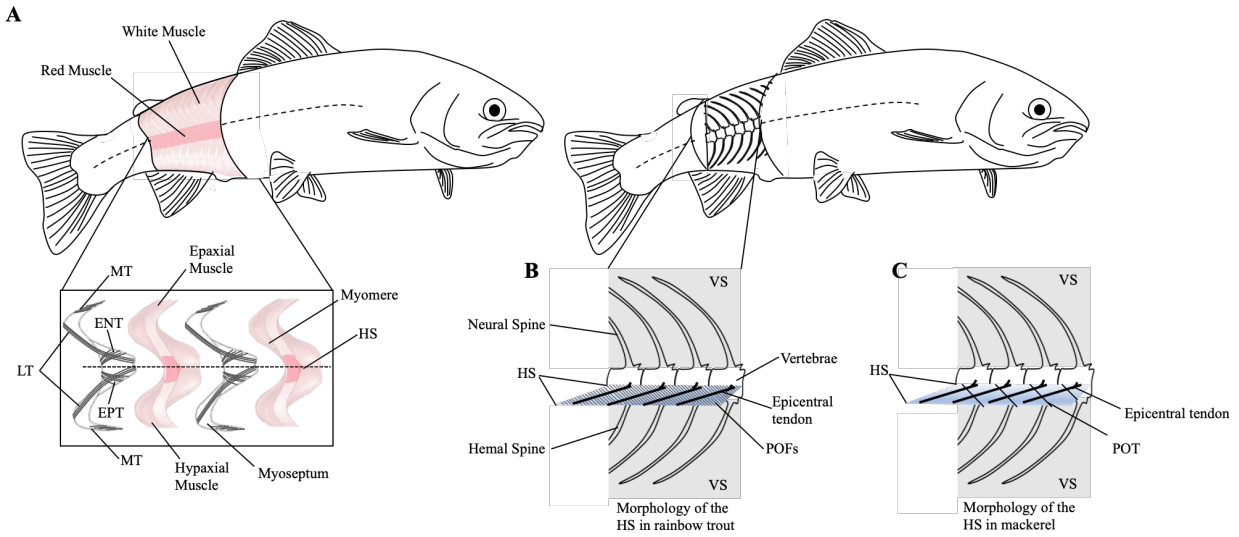

Fig. 1.3. The fish musculoskeletal system. **A**, Fish musculature consists of a series of muscle segments (myomeres) embedded within one another along the length of the fish, on either side of the fish. Adjacent myomeres are separated by a myoseptum. Embedded within the myoseptum of jawed fish are six tendons (two lateral tendons [LT], two myorhabdoid tendons [MT], one epineural tendon [ENT], one epipleural tendon [EPT]). Within most species of fish, red muscle is located on the lateral sides of the fish's body. The horizontal septum divides the myomeres and myosepta into epaxial (dorsal) and hypaxial (ventral) parts. Myosepta schematics modified from Sven Gemballa et al. (2003). **B**, The vertical septum (VS) divides the fish into right and left halves and connects the neural and hemal spines of the vertebrae. The horizontal septum (HS) connects the backbone and skin (not shown) of the fish. Embedded within the horizontal septum of most species of fish are epicentral tendons or epicentral fibers, and posterior oblique tendons or posterior oblique fibers. The horizontal septum of rainbow trout has epicentral tendons and posterior oblique fibers (POFs) (shown). **C**, The horizontal septum (HS) of mackerel has epicentral tendons and posterior oblique tendons (POTs). Note, the bifurcation of epicentral tendons at their distal ends is not shown.

fish and that tendons that can exist as single or double fibrous tracts (Westneat et al., 1993; Westneat & Wainwright, 2001). The authors described the epicentral tendons as splitting into two branches that extend around the laterally-located red muscle—one branch traveling dorsally

and the other, ventrally, and wrapping around the anterior pointing cones of the epaxial and hypaxial myomeres, respectively (Fig. 1.4A). The posterior oblique tendons pass through the sling created by the bifurcated epicentral tendon and attach to the red muscle (Fig. 1.4B). Notably, rainbow trout (personal observation) and other euteleosts (S. Gemballa et al., 2003) differ from mackerel in that their horizontal septum contains posterior oblique fibers, rather than tendons (Fig. 1.3B).

Force Transmission to the Backbone via the Connective Tissue Syncytium

In undulatory swimmers, body undulation is achieved by the anterior-posterior sequential contraction of myomeres (Jayne & Lauder, 1995). As muscles on one side of the fish contract, muscles on the other side relax. Contractile forces generated by the muscles are relayed to the backbone of the fish to cause wavelike bending (Altringham & Ellerby, 1999; Jayne & Lauder, 1995; Syme & Shadwick, 2011). This wavelike bending of the fish's backbone and consequently its whole body, pushes against the water to generate thrust (Altringham & Ellerby, 1999). The tendons identified within the myosepta and horizontal septum are proposed to serve as pathways of force transmission to the backbone of the fish (Sven Gemballa et al., 2003; Sven Gemballa & Vogel, 2002; Westneat et al., 1993; Westneat & Wainwright, 2001). Westneat et al. (1993) propose that the epicentral tendons are put into tension by radially expanding and contracting epaxial and hypaxial muscle. This enables them to behave as struts that keep the posterior oblique tendons in place as they transfer forces generated by contracting red muscle, the muscle type responsible for steady swimming, to the backbone (Fig. 1.4) (Westneat et al., 1993; Westneat & Wainwright, 2001). As rainbow trout lack distinct posterior oblique tendons, it is unclear whether or not the mechanism of red muscle force transfer proposed by Westneat et al. (1993) holds true for this species of fish.

The principle of tension induced alignment dictates that tensile forces along a particular direction cause the alignment of a tissue's extracellular matrix components, such as collagen, in this direction (Paten et al., 2016; Vader, Kabla, Weitz, & Mahadevan, 2009; Voge, Kariolis, MacDonald, & Stegemann, 2008). Although the exact function of the epicentral tendons within the horizontal septum of rainbow trout is unclear—whether they serve a structural purpose (strut) or directly cause bending of the fish's backbone—their existence as bundles of aligned collagen

fibers and their attachment to bone indicate that they experience tensile forces and that they impart these tensile forces onto the bone.

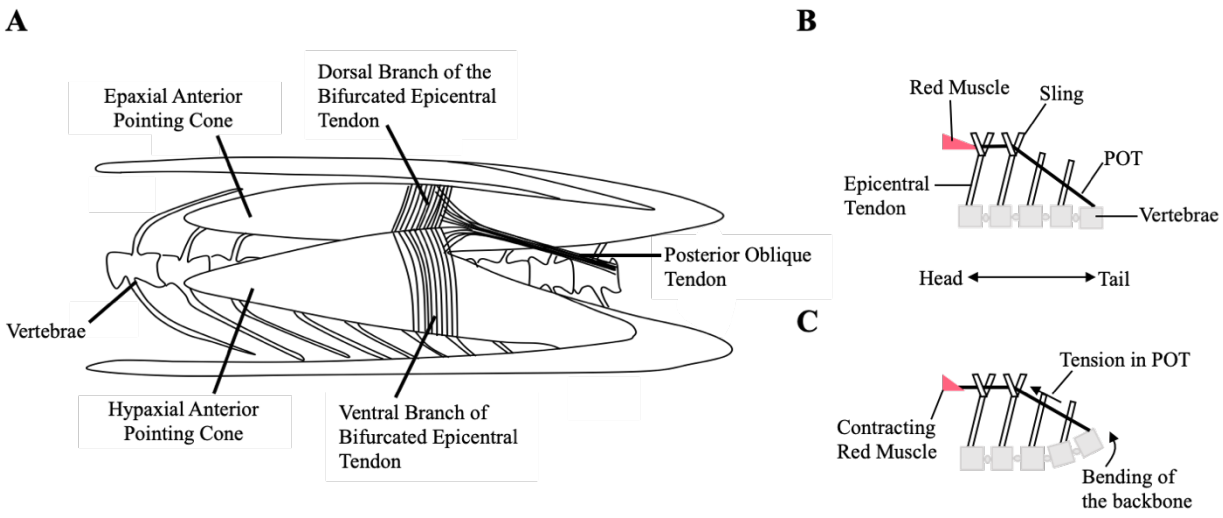

Fig. 1.4. The mechanism of red muscle force transfer to the backbone, proposed by Westneat et al. (1993), for mackerel. **A**, The anatomy of a muscle myomere in mackerel (lateral view). The head of the fish is towards the left. The horizontal septum is located between the epaxial and hypaxial anterior pointing cones. Epicentral tendons embedded within the horizontal septum extend laterally towards the skin (not shown) and bifurcate. Each branch of the bifurcation extends around the laterally-located triangular red muscle (not shown). One branch of the bifurcation travels dorsally, around the epaxial anterior pointing cone. The other branch travels ventrally, around the hypaxial anterior pointing cone. Schematic modified from Westneat et al. (1993). **B**, A dorsal view of the vertebrae, epicentral tendons, posterior oblique tendons, and red muscle, all found on the right side of a mackerel. The posterior oblique tendons (POTs) pass through the slings created by the bifurcating epicentral tendons and attach to red muscle. Schematic modified from Westneat et al. (1993). **C**, The same dorsal view of the vertebrae, epicentral tendons, posterior oblique tendons, and red muscle in mackerel as in **B**. Upon red muscle contraction, the POT is put into tension and is held in place by the epicentral tendon's sling. In this way, the POT transmits force generated by the contracting red muscle to the backbone, which causes its bending. Schematic modified from Westneat et al. (1993).

Purpose of the Study, Objectives, Hypotheses, and Predictions

Studies of the microstructure of tendon-bone attachments in vertebrates have shed light on their function in mediating efficient force transfer between tendon and bone, while dissipating mechanical stresses at the tendon-bone attachment site. Furthermore, tendon-bone attachments have been shown to undergo remodeling in response to novel force regimes, which can influence their function. Gross anatomical studies in fish have been conducted in an attempt to uncover pathways of force transmission via the connective tissue septa to the backbone. However, little focus has been placed on how the connective tissue septa—and the fibrous tracts embedded within them—connect to the bone at the microscopic level to achieve force transfer. In addition, whether or not these tendon-bone attachments are capable of responding to novel force regimes by undergoing remodeling remains unknown. Here, we elucidate the microstructure and material properties of the epicentral tendon-vertebra attachment in rainbow trout, as well as study its response to a novel force regime.

In Chapter 2, I set out to characterize the epicentral tendon-vertebra attachment in rainbow trout at the cellular and extracellular matrix level—both qualitatively and quantitatively—as well as measure the material properties of the attachment using tensile-testing. I hypothesized that the epicentral tendon's angle with respect to the vertebral centrum influences the material properties and structural integrity of the attachment during tensile-testing.

In Chapter 3, I set out to study the effect of unloading on the structure, cellularity, and material properties of the epicentral tendon-vertebra attachment by unloading a subset of attachments in rainbow trout. In addition, I set out to study the effect that this unloading would have on the structure, cellularity, and material properties of intact epicentral tendon-vertebra attachments from neighboring regions. I hypothesized that the epicentral tendon-vertebra attachment would respond to unloading. I predicted that unloaded attachments would alter their cellularity and extracellular matrix content and organization, resulting in altered material properties. I also predicted that loaded attachments from neighboring regions would alter their mechanical behavior to compensate for the unloading of a subset of attachments, as well as their cellularity, extracellular matrix content and organization, and material properties. In this chapter, I present and discuss the material properties testing findings, and discuss my predictions for the histological data in the discussion of Chapter 4.

In Chapter 4, I discuss the overall impact of my thesis work and possible future directions.

CHAPTER 2.

The microstructure and material properties of the epicentral tendon-vertebra attachment in rainbow trout

ABSTRACT

Studies of the microstructure of tendon-bone attachments in mammals have elucidated their role in mediating efficient force transfer between tendon and bone, and in dissipating mechanical stresses. In fish, a contiguous network of connective tissues (skin, septa) surrounding the muscle segments (myomeres) is proposed to be responsible for the transmission of muscle contractile forces to the backbone. A great deal of gross anatomical work has been done to uncover pathways of force transmission to the backbone via the connective tissue septa, however, very little is known about how these septa connect to the bone at the microscopic level to achieve force transfer. We characterized the epicentral tendon-vertebra attachment found within the horizontal septum of rainbow trout at the microscopic level and conducted tensile-testing on attachments found at different positions within the region spanning the dorsal and adipose fin. Tendon collagen fibers inserted directly into the cancellous bone of the vertebral centrum and as such, we classified the epicentral tendon-vertebra attachment as being *fibrous*. The vertebral bone's structure and cellularity were as previously described for salmon: cancellous bone of the arcocentrum (overall lower percentage/density, higher cellularity), surrounding lamellar bone of the autocentrum (overall higher percentage/density, lower cellularity). The tendon was wavy in nature and comprised primarily of collagen, both features characteristic of vertebrate tendon. Notably, tendon proximal to the interface had a higher density of rounded cells, whereas tendon distal to the interface had a lower density of elongate cells. Furthermore, tendon collagen fibers observably splayed at the interface and the tendon had a sinuous footprint on the bone. Tensile-testing of attachments revealed rostral-to-caudal trends in attachment material properties, and tendon angle with respect to the centrum during tensile-testing influenced the material properties and structural integrity of attachments. The latter finding suggests that attachments may be optimized to transfer force along particular angles, as opposed to a large range of angles.

2.1 | INTRODUCTION

Proper biomechanical functioning of the vertebrate musculoskeletal system requires the transfer of forces across tissue interfaces. Muscles are connected to bones either directly (fleshy attachments) or indirectly via tendons (tendinous attachments) (Benjamin, Evans, & Copp, 1986). In tendinous muscle attachments, muscle contractions produce forces, which are transferred across tissue interfaces (muscle-tendon and tendon-bone interfaces) to the skeletal system.

Transfer of force across tissue interfaces where the interacting tissues differ in relative stiffness can generate stress concentrations at the interface, increasing the structure's risk of failure (Benjamin et al., 2002; Genin et al., 2009; Liu et al., 2012; Rossetti et al., 2017; Thomopoulos & Genin, 2013). For example, at the tendon-bone interface in mammals tendons are much less stiff than bone (elastic moduli are ~0.45GPa and ~20GPa, respectively) (Genin et al., 2009; Rossetti et al., 2017). Understanding how tendon and bone interact and connect to one another at the microscopic level to transfer force is critical in understanding musculoskeletal performance and tissue failure.

Two types of tendon-bone attachments have been described at the microscopic scale in mammals: *fibrocartilaginous* and *fibrous* (Benjamin et al., 2002). Fibrocartilaginous tendon-bone attachments consist of a graded transition structure comprised of four zones: 1) tendon; 2) unmineralized fibrocartilage; 3) mineralized fibrocartilage and 4) bone (Benjamin et al., 2002). Fibrous tendon-bone attachments, on the other hand, consist of dense fibrous connective tissue and lack a fibrocartilaginous transition zone between tendon and bone (Benjamin et al., 2002). There are direct and indirect fibrous tendon-bone attachments, where tendon fibers project directly into the bone, or indirectly into the periosteum which then is attached to the bone (Benjamin et al., 2002). Fibrocartilaginous tendon-bone attachments are well described in the mammalian literature as playing a major role in the dispersal of mechanical stress at the junction between flexible tendons and rigid bones. Splaying, unraveling and interdigitation of collagen fibers within the fibrocartilage in proximity to the bone, as well as graded mineralization, are features described as mediating effective load transfer across the fibrocartilaginous Achilles tendon-bone attachment (Rossetti et al., 2017). Unlike fibrocartilaginous tendon-bone

attachments, very little is known about fibrous tendon-bone attachments outside of their basic structure as they are not common in mammals (Apostolakos et al., 2014; Benjamin et al., 2002).

Both fibrocartilaginous and fibrous tendon-bone attachments have been identified and described microscopically in non-mammals such as birds (Hieronymus, 2006; Suzuki et al., 2003), and other reptiles (lizards [Hieronymus, 2006; Suzuki et al., 2002], crocodiles [Suzuki et al., 2003], turtles – identification only [Pereyra et al., 2019]). Mineralized collagen fibers within the bones of extinct fish have been used as evidence for the presence of fibrous tendon-bone attachments (Sanchez et al., 2013); however, the cellular and extracellular microstructure and function of tendon-bone attachments in fish is not well quantified (Rønning et al., 2017). In our experiments, we identified numerous fibrous tendon-bone attachments (epicentral tendon-vertebra attachments, see below) along the backbone of rainbow trout, which suggests that trout may provide an excellent model to learn more about the cellular and extracellular microstructure and function of this unusual type of attachment.

Fish have complex musculoskeletal systems in which body undulation is achieved by the anterior-to-posterior sequential contraction of muscle units, or myomeres, nested within one another along the length of the fish (Alexander, 1969; Jayne & Lauder, 1995). Proposed mechanisms of myomere contractile force transmission to the backbone to cause bending and achieve body undulation involve the contiguous network of connective tissues surrounding the myomeres (myosepta, horizontal septa, vertical septum and skin) that experience tension when muscles contract and expand radially (S. Gemballa et al., 2003; J. H. Long, Adcock, & Root, 2002; J. Long, Hale, Mchenry, & Westneat, 1996; Westneat et al., 1993; Westneat & Wainwright, 2001). The horizontal septum is a connective tissue sheet of particular importance. It connects the vertebral column to the skin, separating the dorsal and epaxial muscles from the ventral hypaxial muscles (S. Gemballa et al., 2003; Westneat et al., 1993; Westneat & Wainwright, 2001) (Fig. 2.1B). Within most species of fish, such as rainbow trout, embedded within the horizontal septum are a series of epicentral tendons that connect to each vertebral centrum and extend laterally towards the skin (S. Gemballa et al., 2003; Westneat et al., 1993; Westneat & Wainwright, 2001). The angle of the epicentral tendon with the long axis of the spine increases towards the posterior part of the fish and tendons can exist as single or double fibrous tracts (Westneat et al., 1993; Westneat & Wainwright, 2001) (Fig. 2.1). In preliminary dissections of rainbow trout, the epicentral tendons split into two fibrous tracts and extended

around the laterally-located, triangular red muscle (as seen in scombrids [Westneat et al., 1993; Westneat & Wainwright, 2001]). In scombrids, one fibrous tract of the bifurcated tendon is described as traveling dorsally and the other ventrally, as each wraps around the anterior pointing cones of the epaxial and hypaxial myomeres, respectively, and projects into the vertical septum (Westneat et al., 1993; Westneat & Wainwright, 2001). Westneat et al. (1993, 2001) suggest that the epicentral tendons are put into tension by the radially-expanding and contracting epaxial and hypaxial anterior pointing cones (Westneat et al., 1993; Westneat & Wainwright, 2001). The principle of tension induced alignment dictates that the alignment of a tissue's extracellular matrix components along a particular direction occurs in response to tension along said direction (Paten et al., 2016; Vader et al., 2009; Voge et al., 2008). Therefore, while the exact role of epicentral tendons (bundles of aligned collagen fibers) in the biomechanical functioning of the fish musculoskeletal system during swimming is unclear—whether they directly cause bending of the backbone, or serve a structural purpose, such as a strut (Westneat et al., 1993; Westneat & Wainwright, 2001)—their existence within the horizontal septum suggests that tensile forces are focused along them and their attachment to bone is indicative that the bone is at the receiving end of the tensile forces.

While a lot of gross anatomical work has been done to try and understand pathways of force transmission to the backbone via the connective tissue sheets surrounding the muscle, very little is known about how these sheets connect to the bone at the microscopic level. Studies of the microstructure of fibrocartilaginous attachments in mammals have elucidated their importance in dissipating stress concentrations and in mediating efficient force transfer between materials with very different material properties. Understanding how the connective tissue sheets connect to the bone of the axial skeleton at the cellular and extracellular matrix level in fish is important in understanding how force transfer to the backbone is achieved. The objectives of this study were two-fold. First, we wanted to characterize the epicentral tendon-vertebra attachment qualitatively and quantitatively at the cellular and extracellular matrix level. Second, we wanted to measure the material properties of the attachment using tensile-testing. We hypothesized that tendon angle with the vertebral centrum would influence the material properties and structural integrity of the attachment during tensile-testing.

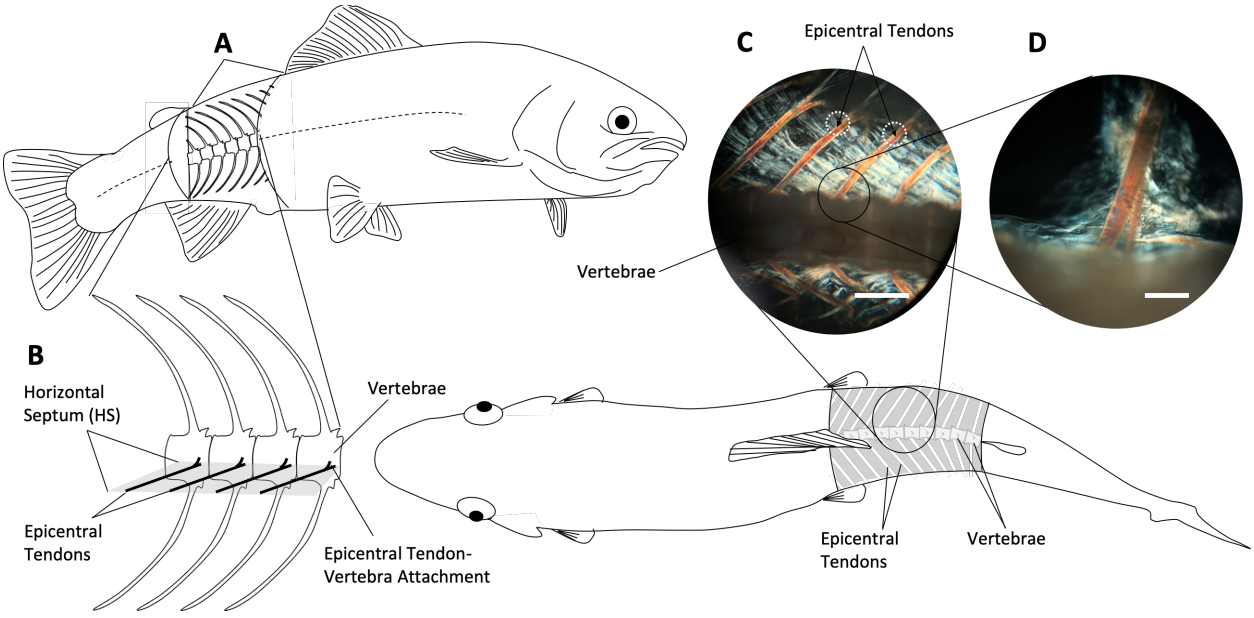

Fig. 2.1 The arrangement of the epicentral tendons within the horizontal septum of rainbow trout and their attachment to vertebrae. **A**, schematic illustrating the region of interest from which all epicentral tendon-vertebra attachments were obtained for histomorphometric analysis and material properties testing. We refer to this region as the *dorsal-adipose tissue segment*. **B**, a lateral view of epicentral tendon-vertebra attachments on one side of the fish. The distal attachment of the tendons to the skin is not shown. **C**, the dorsal view of a cleared horizontal septum and its epicentral tendons (in orange) from the dorsal-adipose tissue segment of a rainbow trout, visualized with polarized light. The scale bar represents 3.5 mm. **D**, a single dissected epicentral tendon's insertion into a vertebra in rainbow trout, visualized with polarized light. The scale bar represents 1 mm.

2.2 | MATERIALS AND METHODS

The study took place at the University of Ottawa, between September 2018 and March 2020. *Oncorhynchus mykiss* (rainbow trout) were obtained from Linwood Acres Trout Farm (Campbellcroft, ON, Canada) and were housed in the University of Ottawa's aquatic facility. All fish were euthanized according to University of Ottawa ACVS protocol BL-1926.

Gross Anatomy

Two male *Oncorhynchus mykiss* (20–30 cm total body length) were euthanized and a tissue segment spanning the region between the dorsal and adipose fin (Fig. 2.1A) was excised to define the location of the epicentral tendon in the horizontal septum and its vertebral insertion points on both sides of the fish. Tissue segments were skinned, fixed in 10% buffered formalin for 10 days (9 days at room temperature, 1 day at 4 °C), and cleared using trypsin enzyme solution (30% saturated aqueous sodium borate, 70% distilled water and 0.1 g trypsin enzyme) (Torres & Ramos, 2016) at 34 °C for 25 days. The solution was changed every 3 to 8 days, or 5 times in total. Specimens were transferred to 30% ethanol, and cleared epaxial and hypaxial muscle was trimmed away to expose the horizontal septum. Pictures of the vertebrae, horizontal septum, and epicentral tendons were taken under polarized light (Fig. 2.1CD) using a compound light microscope (Olympus BH-2, Tokyo).

Five fish (all males, total body length 26.5 ± 0.2 cm, total body weight 183.2 ± 4.7 g) were euthanized and the identical tissue segment to above was excised from each. Epaxial muscle was peeled away from each segment and pictures of the exposed epicentral tendons were taken. The angles at which the tendons branched off the spine were measured within and across all tissue segments. Tendons were numbered in the rostral-to-caudal direction; tendon 1 was located closest to the dorsal fin. A tendon angle vs. attachment position plot was created and a quadratic function was fit to the data using RStudio v1.2.5019 (Fig. 2.4A). This quadratic function was used to extrapolate the angle of tendons with respect to the long axis of the spine of other fish used in this study.

Histology

Tissue Preparation and Staining

The dorsal-adipose tissue segment of 3 euthanized rainbow trout (all male; 20–30 cm total body length) were excised and fixed in 10% buffered formalin for over 1 month (9 days at room temperature, 29 days at 4 °C), then decalcified in 10% Tris-ethylenediaminetetraacetic acid solution for 14 weeks (at room temperature). Epaxial muscle was peeled away to reveal the vertebrae and epicentral tendons within the horizontal septum. Samples underwent paraffinization at the University of Ottawa's Histology Core Facility and were subsequently cut into 2 halves along the midsagittal plane to facilitate individual attachment extraction. Epicentral

tendon-vertebrae attachments within the paraffinized tissue segments (left and right sides) were numbered in the rostral-to-caudal direction and 3 attachments were excised from each fish (2 contralateral attachments from position 4 and 1 attachment in the vicinity, in each fish; 9 attachments total). All paraffinized epicentral tendon-vertebra attachments were embedded in Paraplast (McCormick®) and serial sectioned in the rostral-to-caudal direction, in the transverse plane and parallel to the tendon (on the angle with which the tendon inserts into the vertebra; Fig. 2.6B). Five μm thick sections were obtained using a Leica® Jung RM 2035 microtome (Wetzlar, Germany), mounted and stained with Hematoxylin and Eosin (H&E) (see Appendix) for the purpose of histomorphometric analysis.

Epicentral tendon-vertebra attachments that underwent tensile-testing were fixed following tensile-testing in 10% buffered formalin for 3 days, decalcified in 12.5% formic acid solution for 3 days, and underwent the same paraffin processing as untested, or unpulled, attachments. Fixation and decalcification were much shorter time spans as the tendons were already excised from the tissue prior to tensile-testing. A subset (n=10) of tensile-tested attachments from position 4 that were pulled at 45° (n=4) and 90° (n=6) angles were serial sectioned and stained with H&E for the purpose of histomorphometric analysis.

On a single specimen (as viewed in Fig. 2.5), histological sections were stained with Picrosirius Red and Masson Trichrome stains (see Appendix) to better visualize tendon collagen fibers.

Histomorphometric Analyses

- *Areas of Study on the Tendon, Vertebra, and Attachment Site*

Bone structure and cellular density at the tendon to bone attachment site were quantified at 3 points along the anterior to posterior axis of tendon attachment (termed AP regions; APR): the most anterior point of tendon insertion into the vertebra (anterior-posterior region 1; APR1), the most posterior point of tendon insertion defined by adipocyte disruption (anterior-posterior region 3; APR3), and the central and widest point of tendon insertion, equidistant between APR1 and APR3 (anterior-posterior region 2; APR2) (Fig. 2.6A, B). Three serial sections were imaged for each AP region in each analyzed attachment. All sections were imaged at the same brightness and at 13.2x magnification using a compound light microscope (Olympus BH-2, Tokyo). Additional pictures of sections from APR2 were taken at 33x magnification.

For each tissue section imaged at 13.2x magnification, we identified 3 rectangular regions of interest—using ImageJ's rectangle tool—that spanned the medio-lateral (ML) axis of the tendon attachment (medio-lateral regions 1–3; MLR1-MLR3) and used them to quantify changes in bone structure and cellular density within the bone of the vertebrae. MLR1 represented the vertebral bone of the medial portion of the centrum, MLR3 represented the vertebral bone of the lateral portion of the centrum, and MLR2 represented the space directly in between the two (Fig. 2.6A). The dimensions of MLRs were defined based on the size of each tendon attachment. MLR width was determined as the narrowest bone width in APR1 divided by approximately three. This ensured that 3 MLRs could fit across each APR section and that the size of the MLR was constant between sections of a single attachment (Fig. 2.6A). MLR length was made to equal approximate tendon width in APR2; this encompassed the center of the tendon's footprint, excluding the splaying edges of the tendon at the footprint. All MLRs were aligned at the center of tendon attachment and equally spaced in the medio-lateral direction.

For APR2 sections imaged at 33x magnification, two additional MLRs (0.09 mm x 0.09 mm) were positioned on the tendon using ImageJ's rectangle tool, parallel to tendon fiber direction, to quantify cellular density within the tendon (Fig. 2.6A). MLR4 was placed adjacent to the bone and MLR5 was placed distal to the interface (0.376 mm from the lateral border of MLR4). MLRs were positioned along the center of the attachment of one of the tendon's fibrous tracts. Due to a lack of landmarks within the tendon, a constant box size for MLRs 4 and 5 was used across attachments. MLR size was determined as the largest square area to occupy the tendon of MLR5 across all unpulled attachments. Spacing between MLRs 4 and 5 was determined as the largest spacing enabling the positioning of both MLRs within the same image across all unpulled attachments.

- *Bone Percentage Analysis*

The bone percentage within MLR1-MLR3 of all vertebrae sections was quantified by highlighting the bone using ImageJ's color threshold tool (while leaving adipocyte pockets un-highlighted). The highlighted area was then presented as a percentage of total MLR area. ImageJ (NIH, Bethesda, MD) was used to determine optimal brightness settings for bone identification across all APRs of a single attachment. All sections within a single epicentral tendon-vertebra attachment were analyzed under the same brightness settings.

- *Cell Density Analysis*

Cellular density within MLR1-MLR5 of all sections was measured by performing manual cell counts and dividing cell number by the area occupied by the MLR. Hematoxylin-stained nuclei appeared dark purple and were only counted when found inside or touching the MLR box edges. Within the tendon, dark nuclei in plane, and faint nuclei out of plane were counted. Within the bone, nuclei were only counted if they were 1) dark or 2) faint with associated lacunae, to eliminate pilling artifacts within the bone due to cutting.

- *Tendon Footprint Length*

Tendon footprint length, a measure of the sinuosity of tendon attachment to bone, was calculated at APR2 for the length of the MLRs (imaged at 13.2x magnification). The length of the line traced along the attachment of the tendon with the bone was divided by the straight length of the adjacent MLR rectangle to obtain a ratio of *footprint length-to-MLR length* (ImageJ freehand tool; Fig. 2.2.). A ratio of greater than 1 implies that the footprint takes a curved path and that tendon fibers project into the bone over a larger area; a ratio equal to 1 implies that the footprint takes a straight path.

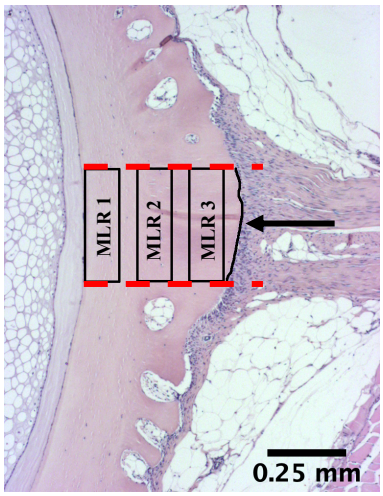

Fig. 2.2. Methodology for measuring the length of the epicentral tendon's footprint on the vertebra. All 13.2x-magnification images of tissue sections from APR2 in unpulled attachments were opened in image J and their designated bone structure analysis MLRs (1–3) were superimposed. Using the freehand line tool in image J, the tendon's footprint in each picture was traced (see arrow). The traced lines spanned the lengths of the MLRs (distance between the red dashed lines).

Material Properties Testing of the Epicentral Tendon-Vertebra Attachment

We were interested in quantifying the material properties of epicentral tendon-vertebra attachments within the dorsal-adipose tissue segment. Twenty-three rainbow trout (4 females, 19 males; total body length 27.22 ± 0.2 cm, total body weight 203.1 ± 4.5 g) were euthanized and the dorsal-adipose tissue segment was excised from each. Every second epicentral tendon-vertebra attachment (4-6 attachments per fish, positions 2, 4, 6, 8, 10, 12, and alternating between left and right sides) was excised from each dorsal-adipose tissue segment, immediately added to 1X tris-buffered saline, and was tensile-tested within 30 minutes. Each epicentral-vertebra attachment was subjected to tensile-testing once, by pulling on the vertebra with the tendon positioned on one of 2 angles with respect to the vertebral column's long axis: 45° or 90° (Fig. 2.3). Epicentral tendons were gripped at a distance of ~2 mm from the vertebra and attachments were tensile-tested at a speed of 5 mm/min using an Instron® 3000 Universal Tester

(Norwood, MA), together with Bluehill® 2 software. A speed of 5 mm/min allowed for a sufficient number of data points to be collected per mm of tissue elongation (~1200 data points per mm of tissue elongation) as attachments only extended a few mm before failing, which made it easier to filter out artificial signals, or noise. Vertebra grips were added as extensions to the apparatus' top moving grip, while a spring clamp and C-clamp served as a tendon-gripping extension to the bottom fixed grip (Fig. 2.3). Force (N) vs. Elongation (mm) data was smoothed (LOESS) to reduce machine noise and normalized to a baseline of 0 using MATLAB® R2019b (Natick, MA). The following material properties were extracted from the curves using MATLAB® R2019b (Natick, MA): maximum load (N) and maximum extension (mm). Trials in which the tendon slipped through the bottom gripper or was too short to be grabbed by the bottom gripper were discarded.

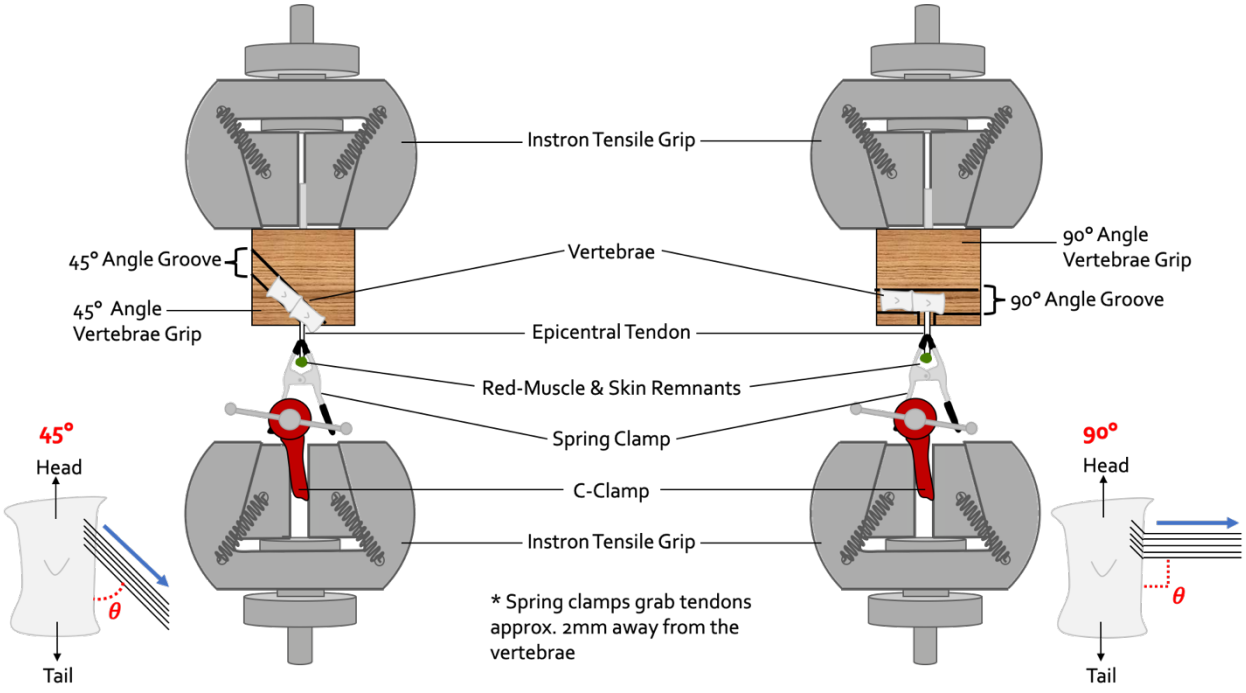

Fig. 2.3. Schematics illustrating the tensile-testing apparatus setups. Attachments were tensile-tested with the tendons positioned on one of two angles relative the long axis of the vertebrae: 45° or 90°.

Analyses of Tensile-Tested Attachments

Tissue sections from APR2 of 10 tensile-tested attachments (45°-pulled, n=4; 90°-pulled, n=6) were imaged to quantify bone and cell density using the histological techniques above. Placement of MLRs was done in a similar fashion to that listed above but due to damage incurred by the tendon during tensile-testing, position of APR1 and APR3 were less clear, possibly adding variation in the placement of APR2. For consistency, MLR1-3 widths were calculated based on the average ratio of bone-width to MLR-width for unpulled specimens in APR2. Once MLR width was set, MLR1-3 lengths were then calculated based on the average ratio of MLR-length to MLR-width from unpulled specimens. Being that a large portion of tendon was absent across all APRs, cellular density was measured within MLR1-MLR4 only. Due to tendon damage, MLR4 was placed in the most intact-remaining portion of tendon next to the bone.

Statistical Analysis

All statistical analyses were conducted by performing linear mixed effects modeling and Bonferroni *post hoc* analyses using RStudio v1.2.5019, with the exception of the tendon angle analysis in which a quadratic regression model was used to estimate tendon angles with respect to the long axis of the spine (see Tables 2.2, 2.4, 2.6 and 2.8 for summaries of models used). The presented models always included the fixed effects of interest, regardless of their significance. In no case were additional fixed effects (weight, length, sex, side of the fish) significant—as determined by model comparisons and in the final model itself—and therefore, these effects were not included in the presented models for simplicity. Heteroscedasticity of fixed effects was corrected using the *VarIdent* function in RStudio. p values of less than 0.05 were considered statistically significant. All values were presented as means ± standard error of the means. All values calculated using the linear mixed effects models were presented as estimated marginal means.

Contributions of Other Authors: Cassandra Donatelli conducted material properties testing on attachments isolated by Emily MacMaster and applied data transformations. Cassandra also applied a curve of best fit to the tendon angle vs. tendon attachment position data.

2.3 | RESULTS

Gross Anatomical Dissection

In a quantitative analysis of 5 rainbow trout (total body length 26.5 ± 0.2 cm, total body weight 183.2 ± 4.7 g), we found epicentral tendon angle within the dorsal-adipose tissue segment increased as tendon attachment position approached the tail (Table 2.1–2.2; Fig. 2.4A). Using a quadratic regression model to fit a curve of best fit to the data (Table 2.2), the angles of tensile-tested tendons at different positions with respect to the long axis of the spine were estimated to be: 41.9 ± 1.5° (position 2); 44.2 ± 1.2° (position 4); 50.3 ± 1.0° (position 6); 60.3 ± 0.9° (position 8) and 74.1 ± 1.1° (position 10), with tendon attachment positions numbered in the rostral-to-caudal direction.

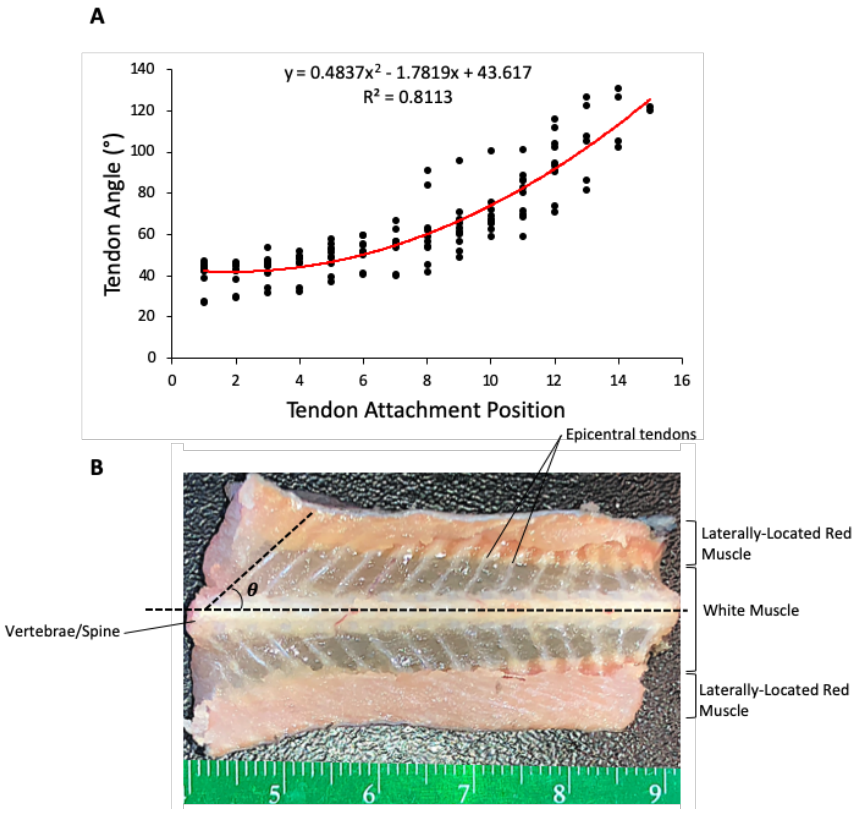

Fig. 2.4. Quantitative analysis of the angles that tendons make with the long axis of the spine, within the dorsal-adipose tissue segment of rainbow trout. **A**, the relationship between tendon angle and tendon attachment position within the dorsal-adipose tissue segment of 5 rainbow trout. Tendon angles on both sides of the fish were measured using ImageJ. Tendon attachments were numbered in the rostral-to-caudal direction. A lower tendon attachment position value represents attachments found more rostral, while a higher tendon attachment position value represents attachments found more caudal. A quadratic function was fit to the data using Rstudio v1.2.5019 and was used to determine the angle of tendons with respect to the long axis of the spine. **B**, a dorsal view of the epicentral tendons within the dorsal-adipose tissue segment of a rainbow trout. The head of the fish is towards the left, the tail of the fish is towards the right. Note that the red muscle is hidden under epaxial white muscle.

Table 2.1. Estimated tendon angle ± standard error of the estimate as a function of tendon attachment position within the dorsal-adipose tissue segment. Tendon angles were estimated using the polynomial regression model in Table 2.2.

Tendon Attachment Position	Tendon Angle
2	41.9 ± 1.5°
4	44.2 ± 1.2°
6	50.3 ± 1.0°
8	60.3 ± 0.9°
10	74.1 ± 1.1°

Table 2.2. Model summary and ANOVA results for the quadratic regression model used in the tendon angle analysis of unpulled epicentral tendon-vertebra attachments. $\alpha = 0.05$. The p-values of significant predictors ($p < 0.05$) are in bold.

Model: Response Variable	Tendon Angle			
	num DF	den DF	F	*P*
Fixed Effects† :				
Tendon Attachment Position	1	129	3.44	0.0660
I(Tendon Attachment Position ^2)	1	129	57.55	**<0.0001**

† In model comparisons, the second-degree polynomial regression model was determined to best fit the data. Side was not a significant fixed effect and therefore data from both sides of the fish was pooled. Tendon attachment position was treated as a continuous variable in this analysis.

Histological Analysis of the Epicentral Tendon-Bone Attachment

Qualitative Observations

At the epicentral tendon-vertebra interface, individual tendon fibers projected directly into the bone (arrows in Fig. 2.5A'') and continuations of these fibers were visible within the bone (Fig. 2.5D'). The tendon's footprint on the vertebra appeared to take a sinuous path (Fig. 2.5).

Tendon appeared rich in unmineralized collagen and when Picrosirius Red-stained sections were viewed under polarized light, it exhibited a wavy structure in proximity to the interface (Picrosirius Red stained all collagen red, Fig. 2.5B/C, B'/C'; Masson Trichrome specifically stained *unmineralized* collagen blue, Fig. 2.5D, D'). Bone tissue appeared to contain mineralized collagen stained red with Masson Trichrome (Fig. 2.5D, D').

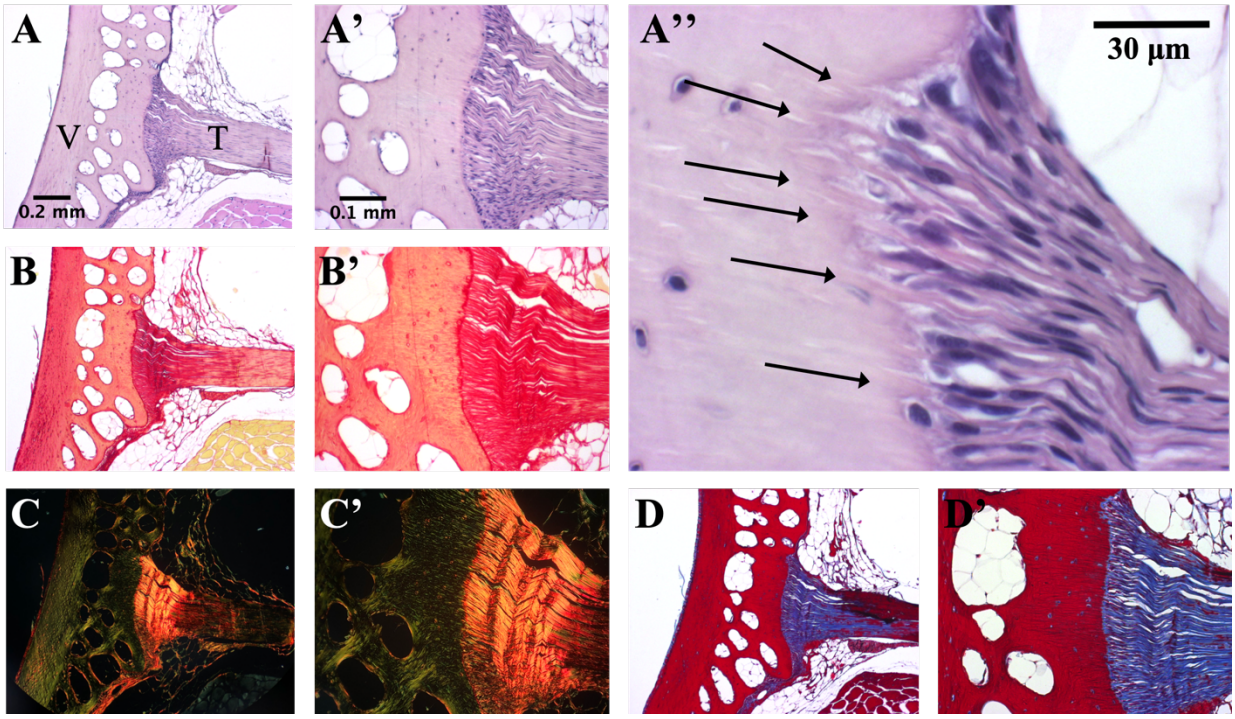

Fig. 2.5. Three serial sections from APR2 of an epicentral tendon-vertebra attachment stained with H&E, Picrosirius Red and Masson Trichrome stains, and visualized at different magnifications (13.2x, 33x and 132x). The dorsal-adipose tissue segment of a rainbow trout (male; 30–35 cm TBL) was excised and fixed in 10% buffered formalin for over 1 month (9 days at room temperature, 29 days at 4 °C), decalcified in 10% Tris-ethylenediaminetetraacetic acid solution for 2 months (at room temperature). Epaxial muscle was peeled away to reveal the vertebrae and epicentral tendons within the horizontal septum. Samples were paraffinized at the University of Ottawa's Histology Core Facility and were subsequently cut into 2 halves along the midsagittal plane. One attachment from position 1 was excised. The attachment was embedded in Paraplast (McCormick®) and serial sectioned in the rostral-to-caudal direction, in the transverse plane and parallel to the tendon. Five µm thick sections were obtained using a microtome. Three serial sections from APR2 were selected for staining. **A**, **A'**, **A''**, micrographs of the first serial section, stained with H&E and imaged under non-polarized white light at 13.2x, 33x and 132x magnification, respectively. A subset of tendon collagen fibers penetrating the bone are labeled in **A''** (arrows). **B**, **B'**, **C**, **C'**, micrographs of the second serial section, stained with Picrosirius Red and imaged at 13.2x and 33x magnifications. **B**, **B'**, were imaged using non-polarized white light; **C**, **C'** were imaged using polarized white light. **D**, **D'**, micrographs of the

third serial section, stained with Masson Trichrome and imaged under non-polarized white light at 13.2x and 33x magnification, respectively. See **A** for the scale bar of all 13.2x magnification micrographs and **A'** for the scale bar of all 33x magnification micrographs. The vertebra (V) is located to the left of the micrographs, while the tendon (T) is located towards the right. Abbreviations: APR, anterior-posterior region

Quantitative Observations

Mean bone percentage and mean cellular density varied depending on the distance from the tendon-bone interface (ML region) and the anterior to posterior position along the tendon to bone attachment (AP region) (Tables 2.3–2.4; Fig. 2.6).

- *Bone Percentage Along the Anterior-Posterior Axis*

Mean bone percentage tended to decrease towards the posterior of the attachment. Specifically, mean bone percentage tended to decrease in proximity to the tendon attachment site (Table 2.3; Fig. 2.6C). Adjacent to the interface (MLR3), mean bone percentage was significantly lower within the posterior portion of the attachment (APR1&2 > APR3, $p < 0.05$). Moving away from the interface (MLR2), mean bone percentage was significantly lower within the central and posterior portions of the attachment (APR1 > APR2&APR3, $p < 0.05$). Farthest from the interface (MLR1), there were no significant differences in mean bone percentage across AP regions ($p > 0.05$).

- *Bone Percentage Along the Medio-Lateral Axis*

Differences in mean bone percentage that occurred along the medio-lateral axis depended on position along the anterior-posterior axis (APR) (Table 2.3; Fig. 2.6C). At the anterior portion of the tendon attachment (APR1), mean bone percentage was greatest distal to the interface (MLR1&2 > MLR3, $p < 0.05$). At the central portion of the tendon attachment (APR2), mean bone percentage did not differ along the medio-lateral axis of the attachment ($p > 0.05$). Within the posterior portion of the attachment (APR3), mean bone percentage was significantly greatest farthest from the interface (MRL1 > MLR2&3, $p < 0.05$).

- *Bone Cellular Density Along the Anterior-Posterior Axis*

Mean bone cellular density along the anterior-posterior axis was variable (Table 2.3; Fig. 2.6D). At the interface (MLR3), mean bone cellular density was significantly lower within the posterior portion of the attachment (APR1&2 > APR3, $p < 0.05$). Moving away from the interface (MLR2), mean bone cellular density was highest at the central portion of the tendon attachment (APR2 > APR1&3, $p < 0.05$). Farthest from the interface (MLR1), there were no significant differences in mean bone cellular density across AP regions ($p > 0.05$).

- *Bone Cellular Density Along the Medio-Lateral Axis*

Mean bone cellular density tended to be greatest in proximity to the interface. At the anterior portion of the tendon attachment (APR1), mean bone cellular density was greatest close to the interface (MLR1&2 < MLR3, $p < 0.05$; Table 2.3; Fig. 2.6D). Along the central medio-lateral axis of the tendon attachment (APR2), mean bone cellular density showed a similar pattern of being greatest closer to the interface (MLR1 < MLR2&3, $p < 0.05$). At the posterior portion of the tendon attachment (APR3), mean bone cellular density did not differ significantly along the medio-lateral axis of the tendon attachment ($p > 0.05$), however, cellular density within MLRs 2 and 3 was 35% and 27% greater in comparison to that of MLR1.

- *Tendon Cellular Density Along the Medio-Lateral Axis*

Along the central medio-lateral axis of the tendon attachment (APR2), mean cellular density of tendon was higher than that of bone (for all ML regions compared, $p < 0.05$; Table 2.3; Fig. 2.6E). Within the tendon, cellular density was greatest in proximity to the interface (MLR4 > MLR5, $p < 0.05$).

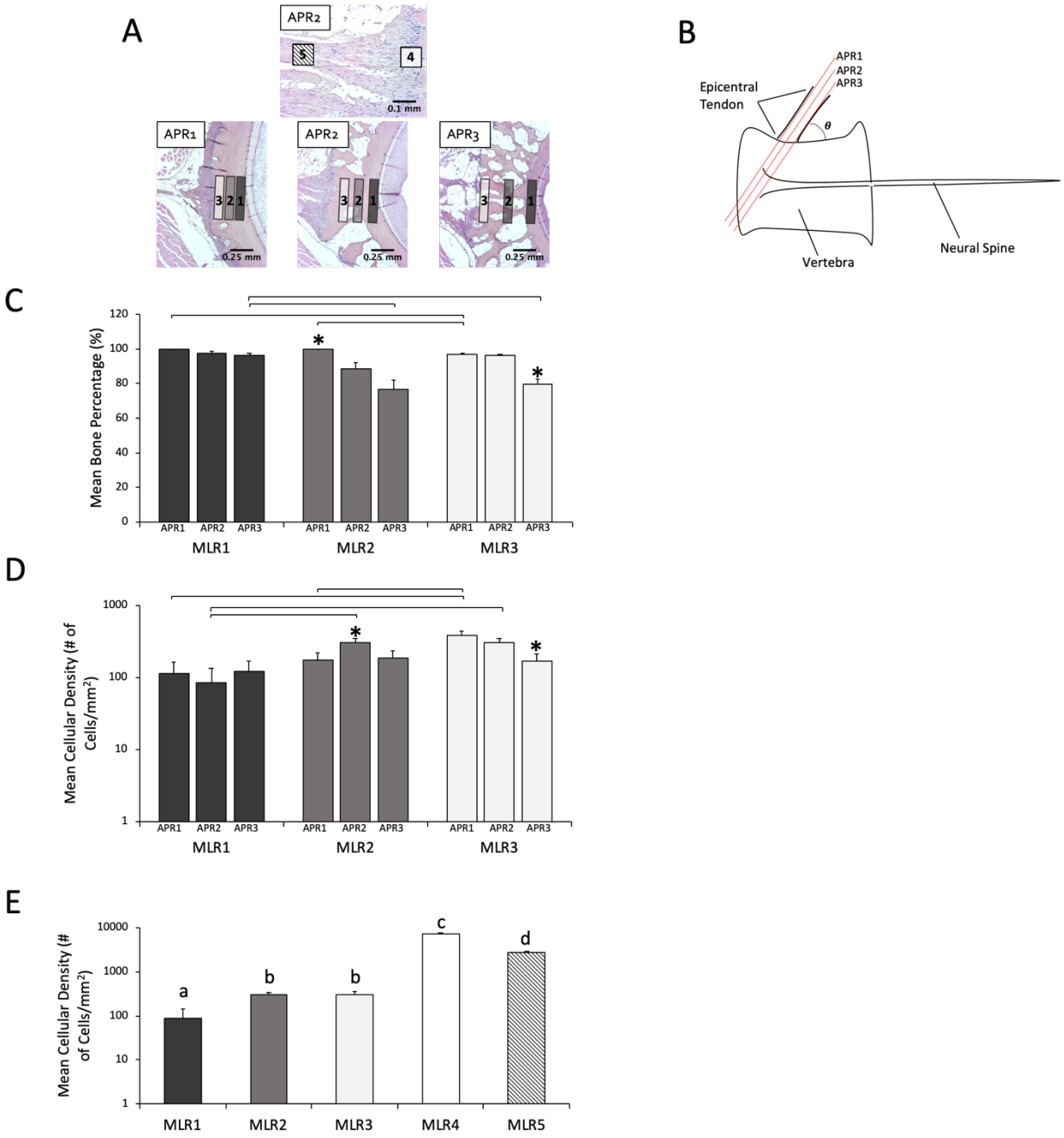

Fig. 2.6. Histomorphometric analyses of the epicentral tendon-vertebra attachment. Epicentral tendon-vertebra attachments within tissue segments (left and right sides) were numbered in the rostral-to-caudal direction and 3 attachments were excised from each fish (2 contralateral attachments from position 4 and 1 attachment in the vicinity, in each fish; 9 attachments total). **A**, Three H&E-stained serial sections were imaged for each of the AP regions for each attachment analyzed. All mounted sections were imaged at 13.2x magnification. Additional

pictures of sections from APR2 were taken at 33x magnification. Three rectangular regions of interest that spanned the medio-lateral axis of the tendon attachment (MLR1-MLR3) were positioned within the bone of each section imaged at 13.2x magnification. Two additional MLRs were positioned on the tendon (MLR4, MLR5) of sections imaged at 33x magnification. **B**, dorsal view of a vertebra and epicentral tendon; the head of the fish is towards the left, the tail is towards the right. The orientation of the red dashed lines indicates the plane in which histological sections were obtained. Each dashed line defines an AP region. **C**, quantification of bone within MLRs1-3 of all sections using Image J's (NIH, Bethesda, MD) color threshold tool to highlight the bone. Highlighted area is presented as a percentage of the total MLR area. **D**, quantification of cellular density within the bone (MLR1-3) of all sections by performing manual cell counts and dividing the cell number by the area occupied by the MLR. **E**, quantification of cellular density along the tendon-bone attachment (MLRs1-5) with APR2 of all sections by performing manual cell counts and dividing cell number by the area occupied by the MLR. Significant differences ($p < 0.05$, Bonferroni *post hoc*) are denoted by different letters. Within **C** and **D**, brackets denote significant differences ($p < 0.05$, Bonferroni *post hoc*) in mean bone percentage and mean cellular density between the different MLRs of a given APR. Stars (*) denote significant differences ($p < 0.05$, Bonferroni *post hoc*) in mean bone percentage and mean cellular density between the same MLR of different APRs. Stars indicate a mean that is significantly different from all others. Estimated marginal means calculated using the LME models (Table 2.4) ± SE are presented. $\alpha = 0.05$. Abbreviations: APR, anterior-posterior region; MLR, medio-lateral region

Table 2.3. Estimated marginal means ± standard errors of bone percentage and cellular density as a function of MLR and APR within unpulled epicentral tendon-vertera attachments. Estimated marginal means ± SE were calculated using the linear mixed effects models used in the bone percentage and cellular density analyses of unpulled epicentral tendon-vertebra attachments (Table 2.4). Abbreviations: MLR, medio-lateral region; APR, anterior-posterior region

		MLR1	MLR2	MLR3	MLR4	MLR5
Bone Percentage	**APR1**	99.5 ± 0.2	99.6 ± 0.3	96.8 ± 0.8	-	-
	APR2	97.6 ± 1.1	88.8 ± 3.2	96.0 ± 1.1	-	-
	APR3	96.5 ± 1.1	76.8 ± 5.1	79.8 ± 2.6	-	-
Cellular Density	**APR1**	114.8 ± 46.5	172.5 ± 46.5	386.5 ± 46.5	-	-
	APR2	85.4 ± 46.5	298.1 ± 46.5	300.1 ± 46.5	7225.5 ± 174.1	2753.3 ± 151.2
	APR3	120.9 ± 46.5	185.6 ± 46.5	165.5 ± 46.5	-	-

Table 2.4. Model summary and ANOVA results for final linear mixed effects models used in the bone percentage and cellular density analyses of unpulled epicentral tendon-vertebra attachments. The p-values of significant predictors ($p < 0.05$) are in bold. Abbreviations: APR, anterior-posterior region; MLR, medio-lateral region

Analysis	Bone structure analysis of untested attachments				Cellular density analysis of untested attachments within bone only (MLR1-3)				Cellular density analysis of untested attachments within APR2 only (MLR1-5)			
Model:												
Response Variable	Bone Percentage				Cellular Density				Cellular Density			
Random Effect	Fish				Fish				Fish			
Nested	Tendon				Tendon				Tendon			
	num DF	def DF	F	*P*	num DF	den DF	F	*P*	num DF	den DF	F	*P*
Fixed Effects:												
MLR	2	226	6.67	**0.0015**	2	226	41.78	**<0.0001**	4	122	521.80	**<0.0001**
APR	2	226	5.32	**0.0055**	2	226	0.73	0.4812	-	-	-	-
MLR x APR	4	226	10.83	**<0.0001**	4	226	13.02	**<0.0001**	-	-	-	-

- *Tendon Footprint Length*

The mean *footprint length-to-MLR length* ratio for tissue sections from APR2 ranged between 1.03-1.34 (1.12 ± 0.04), meaning the tendon's footprint was sinuous.

Material Properties Testing of the Epicentral Tendon-Vertebra Attachment

Maximum Load

Regardless of pull angle, when comparing the mean maximum loads of tendon attachments found in different positions within the dorsal-adipose tissue segment, rostral tendon attachments had higher mean maximum loads compared with attachments closer to the tail (positions 2 and 4 significantly greater than 6, 8 and 10; $p < 0.05$) (Tables 2.5–2.6; Fig. 2.7A).

Regardless of tendon attachment position, attachments tensile-tested on a 45° angle had a significantly larger mean maximum load (0.7 ± 0.1 N) in comparison to those tested on a 90° angle (0.6 ± 0.04 N) (Table 2.6).

Maximum Extension

Regardless of pull angle, when comparing the mean maximum extensions of tendon attachments found in different positions within the dorsal-adipose tissue segment, tendon attachments in position 4 had a significantly lower mean maximum load compared with attachments in positions 2 and 10 ($p < 0.05$) (Tables 2.5–2.6; Fig. 2.7B).

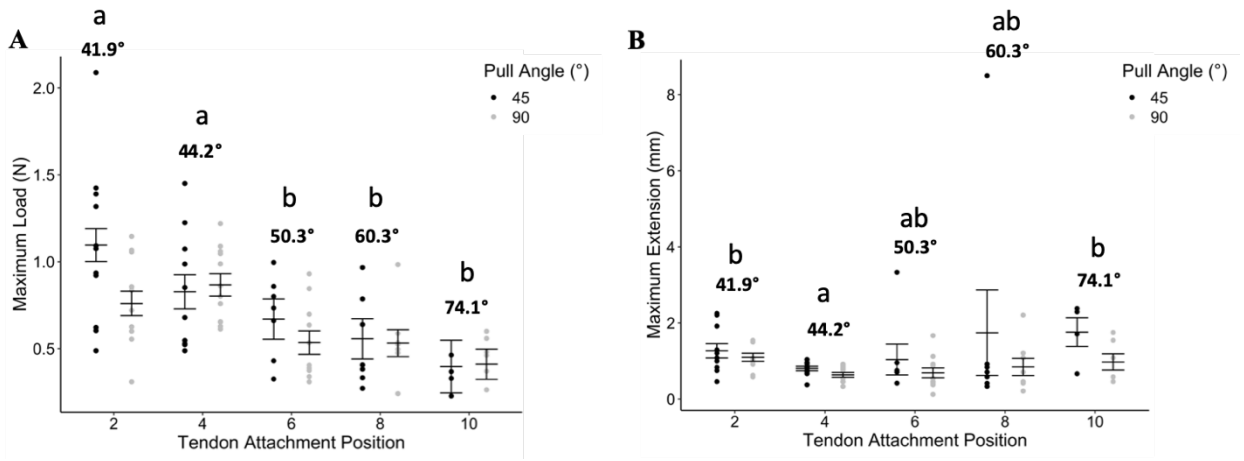

Fig. 2.7. The material properties of epicentral tendon-vertebra attachments within the dorsal-adipose tissue segment. **A**, **B**, graphs comparing the maximum loads (N) and maximum extensions (mm), respectively, experienced by attachments along the length of the dorsal-adipose tissue segment (a lower tendon attachment position value represents tendon attachments found more rostral, while a higher tendon attachment position value represents tendons found more caudal), pulled on both 45° and 90° angles. The natural angle that each tendon makes with the long axis of the spine at a given position within the dorsal-adipose tissue segment (determined using the function in Fig. 2.4A) is indicated above each tendon attachment position. Estimated marginal means ± SE are presented. $\alpha = 0.05$. Tendon attachment positions that share a letter in common are not significantly different (45° and 90°-pulled attachments pooled at each position; $p > 0.05$, Bonferroni *post hoc*).

Table 2.5. Estimated marginal means ± standard errors of maximum loads and maximum extensions as a function of tendon attachment position within the dorsal-adipose tissue segment. Estimated marginal means ± SE were calculated using the linear mixed effects models used in the material properties analyses of epicentral tendon-vertebra attachments (Table 2.6).

Tendon Attachment Position	Pull Angle	Maximum Load (N)	Maximum Extension (mm)
2	45°	1.1 ± 0.1	1.3 ± 0.2
	90°	0.8 ± 0.1	1.1 ± 0.1
4	45°	0.8 ± 0.1	0.8 ± 0.1
	90°	0.9 ± 0.1	0.6 ± 0.1
6	45°	0.7 ± 0.1	1.0 ± 0.4
	90°	0.5 ± 0.1	0.7 ± 0.1
8	45°	0.6 ± 0.1	1.8 ± 1.1
	90°	0.5 ± 0.1	0.8 ± 0.2
10	45°	0.4 ± 0.1	1.8 ± 0.4
	90°	0.4 ± 0.1	1.0 ± 0.2

Table 2.6. Model summary and ANOVA results for linear mixed effects models used in the material properties analyses of epicentral tendon-vertebra attachments. $\alpha = 0.05$. The p-values of significant predictors ($p < 0.05$) are in bold.

Analysis	Material Properties Testing				Material Properties Testing			
Model: Response Variable Random Effects	Maximum Load Fish				Maximum Extension Fish			
	num DF	den DF	F	*P*	num DF	den DF	F	*P*
Fixed Effects:								
Tendon Position	4	54	6.42	**0.0003**	4	54	3.00	**0.0263**
Pull Angle	1	54	8.22	**0.0059**	1	54	0.64	0.4288
Tendon Position x Pull Angle	4	54	1.47	0.2244	4	54	0.61	0.6542

Comparing Cellular Density and Bone Percentage of Tensile-Tested (45°- and 90°-pulled) and Unpulled Attachments Along the Central Medio-Lateral Axis (APR2)

During tensile-testing, the location of failure always occurred within the tendon and never in the bone (Fig. 2.8). Only tensile-tested attachments of position 4 were measured for cellular density and bone percentage (10 fish; 10 attachments) and were compared with unpulled attachments of position 4 (3 fish; 6 attachments).

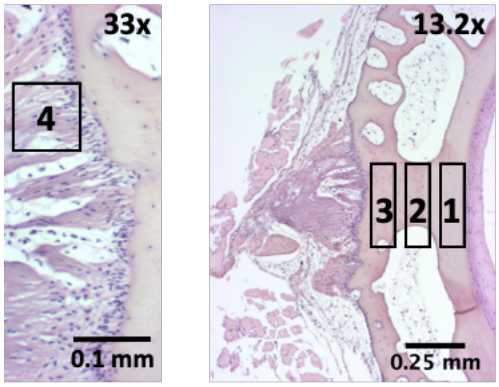

Fig. 2.8. The positioning of MLRs within tissue sections of tensile-tested attachments in histomorphometric analyses. Three H&E-stained serial sections from APR2 were imaged at 13.2x magnification and 33x magnification for each tensile-tested attachment analyzed. Three rectangular regions of interest that spanned the medio-lateral axis of the tendon attachment (MLR1-MLR3) were positioned within the bone of each section imaged at 13.2x magnification. One additional MLR was positioned on the most intact remaining portion of the tendon (MLR4) of each section imaged at 33x magnification. Above is an example of an attachment tensile-tested on a 45° angle.

Bone Percentage Along the Central Medio-Lateral Axis (APR2)

Mean bone percentage along the central medio-lateral axis of the tendon attachment (APR2) did not differ between unpulled, 45°-pulled, and 90°-pulled attachments ($p > 0.05$; Tables 2.7–2.8; Fig 2.9B).

Cellular Density Along the Central Medio-Lateral Axis (APR2)

Along the central medio-lateral axis of the tendon attachment (APR2), mean cellular density within MLR2 of the bone was significantly lower within 90°-pulled attachments in comparison to 45°-pulled attachments ($p < 0.05$) (Tables 2.7–2.8; Fig. 2.9C). Within the tendon (MLR4), mean cellular density was significantly lower within 90°-pulled attachments in comparison to unpulled attachments ($p < 0.05$).

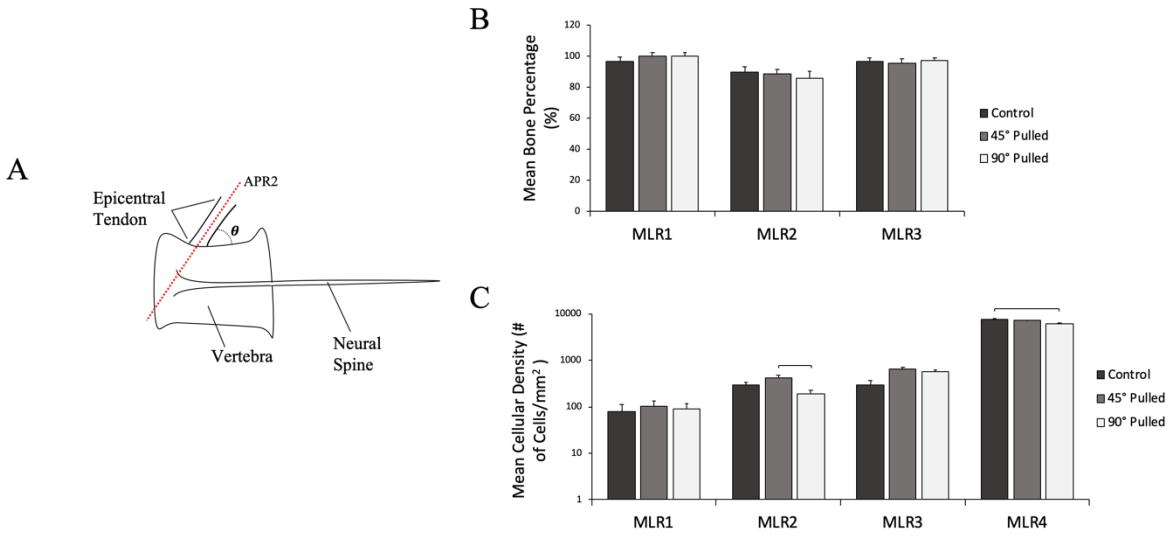

Fig. 2.9. Comparing bone percentage and cellular density of tensile-tested attachments and control (unpulled) attachments to study the effect of tensile-testing on bone percentage and cellular density (proxies for plastic deformation of bone and tendon). **A**, a dorsal view of a vertebra and epicentral tendon; the head of the fish is towards the left, the tail is towards the right. The orientation of the red dashed line indicates the AP region from which histological sections were obtained for comparison: APR2. **B**, **C**, Ten attachments from position 4 of 10 different fish were tensile-tested on 45° (n=4) and 90° (n=6) angles. Attachments originated from both sides of the fish (right side, n=6; left side, n=4). Data was compared to mean bone percentage and mean cellular density data of control attachments from position 4 only (n=6; 2 attachments per fish). Estimated marginal means calculated using the LME models (Table 2.8) ± SE are presented. $\alpha = 0.05$. Brackets indicate $p < 0.05$, Bonferroni *post hoc*. Abbreviations: APR, anterior-posterior region; MLR, medio-lateral region

Table 2.7. Estimated marginal means ± standard errors of bone percentage and cellular density in tensile-tested attachments and control (unpulled) attachments as a function of MLR. Estimated marginal means ± SE were calculated using the linear mixed effects models used in the cellular density and bone percentage analyses of tensile-tested and control (unpulled) attachments (Table 2.8). Abbreviations: APR, anterior-posterior region; MLR, medio-lateral region

		Pull Angle	MLR1	MLR2	MLR3	MLR4
Bone Percentage	**APR2**	**Control**	96.5 ± 2.7	89.8 ± 3.6	96.3 ± 2.5	-
	APR2	**45°**	99.9 ± 2.3	88.3 ± 3.0	95.6 ± 2.7	-
	APR2	**90°**	99.9 ± 2.2	85.6 ± 4.5	97.0 ± 1.9	-
Cellular Density	**APR2**	**Control**	78.2 ± 35.4	293.9 ± 43.6	294.8 ± 62.7	7480.4 ± 239.8
	APR2	**45°**	101.7 ± 33.7	425.3 ± 45.9	634.7 ± 71.7	7071.9 ± 292.4
	APR2	**90°**	89.0 ± 27.5	190.3 ± 37.5	563.2 ± 58.6	6078.7 ± 238.7

Table 2.8. Model summary and ANOVA results for linear mixed effects models used in bone percentage and cellular density analyses of tensile-tested and control (unpulled) attachments. $\alpha = 0.05$. The p-values of significant predictors ($p < 0.05$) are in bold. Only attachments from position 4 were compared. Abbreviations: MLR, medio-lateral region

Analysis	Comparing bone percentage (MLR1-3) between control and pulled attachments				Comparing cellular density within bone and tendon (MLR1-4) between control and pulled attachments			
Model:								
Response Variable	Bone Percentage				Cellular Density			
Random Effect	Fish				Fish			
Nested	Tendon				Tendon			
	num DF	den DF	F	*P*	num DF	den DF	F	*P*
Fixed Effects*:								
MLR	2	122	22.6	**<0.0001**	3	167	219.93	**<0.0001**
Group (Control/45°-pulled/90°-pulled)	2	10	0.58	0.5797	2	10	0.12	0.8918
MLR x Group (Control/ 45°-pulled/90°-pulled)	4	122	1.99	0.1002	6	167	8.59	**<0.0001**

2.4 | DISCUSSION

The Implication of Increasing Tendon Angle with Respect to the Spine

In resting fish, epicentral tendons change angle of attachment with bone as you move posteriorly along the spine (Fig. 2.4); anterior tendons have smaller angles that more closely resemble 45°, while posterior tendons have larger angles that more closely resemble 90°. This increase in tendon angle towards the tail of a resting fish may be related to the increase in body wave amplitude that occurs towards the tail of the fish when it is swimming. As a fish swims, the amplitude of the body wave increases toward the tail. We predict that this change in amplitude stretches the tendon, thus decreasing the angle of tendon's attachment to bone. Although we were not able to measure this, the change in angle may be large enough such that, posterior tendons are in tension when at 45° with respect to the bone.

The Epicentral Tendon-Vertebra Attachment is a Fibrous Attachment

We classified the epicentral tendon-vertebra insertion within rainbow trout as a direct *fibrous* attachment as indicated by the presence of dense fibrous connective tissue and the absence of a fibrocartilaginous transition zone between tendon and bone (Benjamin et al., 2002) (Fig. 2.5). Collagen fibers of the tendon projected directly into the bone, and continuations of these fibers could be seen within the bone (Fig. 2.5A'', D'). These "fibrous continuations" resemble Sharpey's fibers, which have been previously described in the mammalian literature as serving as anchors for tendon, ligament and periosteum connected to bone (Benjamin et al., 2002).

Features of the Vertebral Bone and Epicentral Tendon are Characteristic of What Has Previously been Described for Vertebral Bone and Tendon

We characterized two layers of bone within the vertebrae of rainbow trout. The inner layer consisted of bone whose percentage remained high and unchanged along and anterior-posterior direction, and whose cellular density was lower. The outer layer consisted of bone whose percentage decreased towards the posterior of the attachment and whose cellular density was greater in comparison to that of the inner layer. Nordvik et al. (2005) identified four layers of bone within the vertebrae of salmon, and characterized bone density (comparable to our bone

percentage) and quantified cellular density within each of these layers (Nordvik, Kryvi, Totland, & Grotmol, 2005). Based on their description of these four layers, it is our interpretation that we have quantified bone percentage and cellular density within the autocentrum (layer 3; encompassed by MLR1) and the arcocentrum (layer 4; encompassed by MLRs 2 and 3). The autocentrum is described as a layer of compact lamellar bone with a relatively low osteocyte density, whereas the arcocentrum is described as a layer of cancellous bone with a relatively high osteocyte density (10x higher than that of the autocentrum) (Nordvik et al., 2005). The presence of adipocyte-filled voids within the cancellous bone of the arcocentrum could confer buoyancy to the fish (Bone, 1972; Gray, Kainec, Madar, Tomko, & Wolfe, 2007; R. F. Lee, Phleger, & Horn, 1975). Interestingly, the epicentral tendon inserted directly into the void-filled cancellous bone of the arcocentrum, which lacked a cortex (outer layer of lamellar bone). Previous studies of tendon-bone attachments have described tendons as inserting into the cortices surrounding bones. To our knowledge, this is the first time that the insertion of a tendon into cancellous bone is described at the microscopic level, and the functional implications this may have for a tendon-bone attachment remain unknown.

As has been previously reported for tendon in vertebrates, the epicentral tendon's extracellular matrix was comprised primarily of collagen fibers (Kjaer, 2004; Summers & Koob, 2002), was wavy in nature (Rigby, Hirai, Spikes, & Eyring, 1959; Shah, Nerurkar, Wang, & Galloway, 2015; Suzuki et al., 2002, 2003; Viidik & Ekholm, 1968), and its collagen fibers appeared to splay at the interface, increasing its diameter at the interface (Fig. 2.5, 2.6A) (Benjamin et al., 2002).

Tissue Morphology at the Tendon-Bone Interface—a Result of Mechanical Stimulation?

The structure and cellularity of tendon and bone adjacent to the interface are consistent with the tissues experiencing greater mechanical stimulation within this region, which is to be expected of tissues at tendon-bone interfaces. Although decreases in bone percentage along the anterior-posterior axis of the attachment occurred within bone of the arcocentrum and despite the fact that bone of the arcocentrum is labeled as being cancellous, bone percentage within the arcocentrum remained relatively high in proximity to the interface for a large portion of the attachment and only became significantly trabeculated towards the posterior of the attachment (Fig. 2.6A, C). This feature may confer strength to the attachment by allowing for the anchoring

tendon collagen fibers into the bone and may be a result of higher mechanical stimulation of the bone at the interface, as vertebrate bone has been shown to respond to mechanical stimulation by increasing bone formation in regions of loading (Atkins et al., 2015; Best et al., 2017; Huysseune, Sire, & Meunier, 1994; Saino et al., 2003; Sugiyama et al., 2010; Suniaga et al., 2018; Van Der Meulen, Yang, Morgan, & Bostrom, 2009). Although not quantified, it was observed that within tissue sections from the center of the attachment (APR2), the bone above (dorsal) and below (ventral) the tendon-bone attachment had a greater degree of trabeculation and had open voids on the surface of the bone (Fig. 2.5, 2.6A). This further supports the notion that the relatively high percentage of cancellous bone in proximity to the interface, is a result of higher mechanical stimulation of the bone within this region. In addition, the high cellular density of the bone adjacent to the interface may be a result of mechanical stimulation of the bone within this region as fish bone osteocyte density has been shown to increase in response to mechanical stimulation (Totland et al., 2011) and osteocyte density has been shown to decrease when mammalian bone is not loaded (Aguirre et al., 2006). Alternatively, the higher osteocyte density at the periphery of the vertebrae may be associated with normal bone growth that occurs at the periphery of vertebrae (Totland et al., 2011). Lastly, the epicentral tendon's footprint on the bone was sinuous and tendon fibers observably splayed at the interface. Both are features that could allow for dissipation of force over a larger area and reduce stress concentrations in a region where stresses tend to concentrate (Benjamin et al., 2002; Rossetti et al., 2017). Splaying of tendon fibers has also been proposed to serve as a protective mechanism against slimming of the tendon at the interface, in response to a greater presence of stress concentrations within this region (Benjamin et al., 2002).

The rounded shape and high density of the cells within the tendon in proximity to the interface—in comparison to tendon distal to the interface, which had a lower cellular density and possessed cells with an elongate morphology—further supports the idea that tissues at the interface experience more intense forces than those distal. Although the cells in proximity to the interface have yet to be identified, we predict that these cells may correspond to tenocytes responding to mechanical stimulation. In mammals, tenocytes have been shown to respond to mechanical stimulation by increasing in number, becoming more rounded, as well as increasing the synthesis of extracellular matrix collagen precursors, which has been linked to improved material properties of the tendon (Abraham, Fong, & Scott, 2011; Chicurel et al., 1998;

Heinemeier & Kjaer, 2011; Huisman et al., 2014). High tenocyte activity at the interface could be important for improving the material properties of the epicentral tendon-bone attachment, allowing for more efficient force transfer, while minimizing the risk of tissue failure in a region where mechanical stresses tend to concentrate.

Trends in Material Properties Along the Length of the Dorsal-Adipose Tissue Segment

A decrease in mean maximum load of attachments towards the posterior of the fish (Fig. 2.7A) suggests that tendons may differ in their structure, such as cross-sectional area, and/or composition along the length of the dorsal-adipose tissue segment. Although not uniform, a trend of increasing extension towards the posterior of the fish was also present (Fig. 2.7B). As extension is inversely proportional to cross-sectional area, this data further supports the prediction that tendon cross-sectional area decreased towards the tail.

Attachments May be Optimized to Transfer Force Along Particular Angles

Attachments exhibited different material properties and a different structural integrity when tensile-tested on different angles, suggesting that attachments may be optimized to transfer force along particular angles, as opposed to a large range of angles.

Mean maximum load was greater for attachments tensile-tested on 45° angles in comparison to 90° angles (Fig. 2.7A). Pulling tendons on unnatural angles with respect to the vertebrae may reduce the alignment of tendon collagen fibers, resulting in uneven tendon fiber recruitment and a non-uniform loading pattern within the tendon during tensile-testing. Unequal recruitment of tendon collagen fibers reduces the total cross-sectional area of fibers in tension at a given time, which reduces the maximum tension an attachment can sustain prior to failure.

Bone percentage and bone cellular density served as proxies for permanent bone deformation following tensile-testing. Cellular density within the tendon served as a proxy for permanent tendon deformation following tensile-testing. The difference in cellular density within MLR2 of the bone between 45°- and 90°-pulled attachments (Fig. 2.9C) is likely due to individual differences in cellular density between fish. A difference in cellular density within the bone would be expected if it was accompanied by a difference in mean bone percentage, as osteocytes are embedded within the bone matrix and any displacement of bone would inevitably result in displacement of osteocytes. As bone structure did not differ between 45°- and 90°-

pulled attachments (Fig. 2.9B), cellular density within the bone likely did not differ between 45°- and 90°-pulled attachments as a result of pulling on different angles.

A decrease in cellular density within the tendon at the interface in response to tensile-testing is an indication that the tendon underwent plastic deformation at the interface, resulting in the distancing of tenocytes and/or tenoblasts from one another. While pulling on both angles resulted in plastic deformation of the tendon at the interface, the tendons of 90°-pulled attachments incurred greater plastic deformation at the interface, causing their cellular density to differ significantly from that of control attachments (Fig. 2.9C). Stained histological sections of the epicentral tendon-vertebra attachment revealed that there is continuity of collagen fibers between the tendon and bone, along a straight path, and on the angle that the tendon makes with the vertebral centrum (Fig. 2.5A’’). When the tendon is pulled on an unnatural angle with respect to the bone, alignment of tendon collagen fibers and Sharpay’s fibers within the bone is lost and sharp angles, or corners, are introduced at the tendon-bone interface. It is a well-accepted paradigm in structural engineering that the introduction of corners within a load path generates stress concentrations. Where stress concentrations occur, localized plastic deformation can occur. This paradigm may explain why the tendon adjacent to the interface displays a greater degree of structural integrity when pulled one angle, as opposed to another.

2.5 | CONCLUSION

The epicentral tendon-bone attachment in rainbow trout is a direct fibrous attachment comprised of dense fibrous connective tissue. The vertebral bone examined at the attachment consisted of lamellar bone of the autocentrum (overall higher bone percentage/density, lower cellular density), surrounded by cancellous bone of the arcocentrum (overall lower bone percentage/density, higher cellular density), consistent with previous descriptions of vertebral bone in salmon. To our knowledge, this is the first study to examine a tendon’s direct insertion into cancellous bone lacking a cortex. The epicentral tendon was characteristic of tendons in vertebrates such that it was wavy in nature and its extracellular matrix was primarily composed of collagen. The structure and cellularity of the bone and tendon adjacent to the interface are consistent with tissues experiencing greater mechanical stimulation, which is to be expected of tissues located at tendon-bone interfaces (cancellous bone with relatively high percentage/density and high cellular density; the high density of rounded cells within the tendon; observed splaying

of tendon collagen fibers; sinuosity of the tendon's footprint on the bone). Trends in attachment material properties existed in the rostral-to-caudal direction along the length of the dorsal-adipose tissue segment—an indication that attachment structure and/or composition may differ at different positions along the backbone of the fish. Epicentral tendon angle with respect to the vertebra during tensile-testing influenced the material properties and structural integrity of the attachment, possibly due to uneven tendon fiber recruitment and the generation of stress concentrations at the interface in response to pulling tendons at unnatural angles with respect to the vertebrae. This finding suggests that attachments may be optimized to transfer force along particular angles.

CHAPTER 3.

The effect of unloading on the epicentral tendon-vertebra attachment

ABSTRACT

Tendon-bone attachments in vertebrates have been shown to undergo changes in structure, composition, and material properties, in response to novel force regimes. Macroscopic anatomical studies in fish have described pathways of force transmission to the backbone, via connective tissue septa. Little emphasis has been placed on how these connective tissue septa connect to the bone of the axial skeleton at the microscopic level to achieve force transfer, and whether or not these attachments can undergo remodeling in response to novel force environments, which may affect how they function, remains unknown. We studied the effect of changing load regime on the material properties of epicentral tendon-vertebra attachments in rainbow trout. We induced chronic unloading by severing a subset of epicentral tendons within rainbow trout and allowing for time to pass. Unloading of the epicentral tendon-vertebra attachment had no effect on its material properties after 6 weeks, suggesting that the attachment did not undergo any remodeling, or that remodeling was not sufficient to alter its material properties. This finding suggests that the contiguous network of connective tissues in which the attachments are embedded and the gross anatomy of the epaxial and hypaxial muscle may have supported the maintenance of attachment function, despite local injury.

3.1 | INTRODUCTION

Tendon and bone are two connective tissues known to respond to changing force environments, by altering their cellularity and extracellular matrix content and organization. Consequently, these changes in tissue structure and composition alter tissue material properties. Much of what we know about how vertebrate tendon and bone respond to mechanical stimulation, or lack thereof, has come from studying mammals. Mechanical loading has been shown to result in increased bone formation (Best et al., 2017; Saino et al., 2003; Sugiyama et al., 2010) and increased bone mineral density (and therefore increased stiffness) (Best et al., 2017; Fritton et al., 2005). Unloading of bone has been shown to result in apoptosis of osteocytes (Aguirre et al., 2006), decreased bone mineral density (and therefore decreased stiffness), increased bone resorption, and decreased bone strength (Friedman et al., 2019; Lang et al., 2004; Leblanc et al., 2000). In tendon, tenocytes have been shown to respond to mechanical loading by increasing in number (Andersson et al., 2011), becoming more rounded (Chicurel et al., 1998; Huisman et al., 2014), and increasing the rate at which they secrete extracellular matrix collagen precursors (Huisman et al., 2014)—a response that has been linked to improved material properties of the tendon (Heinemeier & Kjaer, 2011). Increased tendon diameter (Magnusson & Kjaer, 2003, 2019) and increased tendon stiffness (Arampatzis et al., 2010; Magnusson & Kjaer, 2019) have also been reported in tendons subjected to increased mechanical loading. Fibrocartilage formation within regions of tendons subjected to compression (Vogel & Koob, 1989) and the formation of tendon crimp in tendon-like constructs subjected to compression (Herchenhan et al., 2012) have also been observed. Unloading of tendon has been shown to result in decreased tendon stiffness (Magnusson & Kjaer, 2019), decreased tendon strength (Loitz, Zernicke, Vailas, & Kody, 1989), decreased collagen synthesis (De Boer et al., 2007), decreased collagen fiber alignment (Bayer et al., 2014), rounding of tenocytes (Bayer et al., 2014), and decreased tendon cross-sectional area in cases of extreme prolonged disuse (Maganaris et al., 2006).

Bones in fish have been shown to respond to mechanical loading in similar and novel ways (increased bone formation [Atkins et al., 2015; Huysseune et al., 1994; Suniaga et al., 2018]; increased bone mineral density [Totland et al., 2011]; changes in bone morphology [Du & Standen, 2020]; novel increased osteocyte density [Totland et al., 2011]). Unloading of

developing fish tendons has been shown to result in altered tenocyte morphology and decreased synthesis of extracellular matrix (Subramanian et al., 2018). Although little is known about how fish tendons undergo remodeling in response to changes in mechanical loading, tendon morphology (other than its hierarchical organization) and its cellular processes have been shown to be conserved across vertebrate groups (J. W. Chen et al., 2014; Kastelic, Galeski, & Baer, 1978; Shadwick, Rapoport, & Fenger, 2002; Summers & Koob, 2002), and as such, one might expect them to respond in ways similar to those in mammals. Where tendon morphology has been shown to differ between mammals and other vertebrates, however, is at the tendon's attachment to bone (Suzuki et al., 2002, 2003).

Contractile forces generated by skeletal muscle are transferred through tendons. The transfer of force across the tendon-bone interface can generate stress concentrations, as tendon and bone differ vastly in their structure, composition, and material properties (Benjamin et al., 2002). Two main types of tendon-bone attachments have been identified at the microscopic level in vertebrates, namely *fibrocartilaginous* (characterized by a fibrocartilage transition zone between tendon and bone) and *fibrous* (characterized by dense fibrous connective tissue and the absence of fibrocartilage) (Benjamin et al., 2002). Mechanical modeling has shown that fibrocartilaginous tendon-bone attachments play a major role in the dissipation of mechanical stress at the tendon-bone junction (Rossetti et al., 2017). Furthermore, mechanical stimulation has been shown to be important for their maintenance (Deymier et al., 2019), development (Schwartz et al., 2013), and healing (Gilotra et al., 2016), so that they may function efficiently in mediating efficient force transfer from tendon, to bone, while reducing the risk of tissue failure (Deymier et al., 2019). Unloading of healthy tendon-bone attachments can lead to attachment remodeling, namely bone loss and decreased mineral (bioapatite) crystal size and alignment—possibly attributed to decreased collagen alignment, which has been observed in unloaded developing tendon-bone attachment sites (Deymier et al., 2019; Schwartz et al., 2013). These structural alterations change the attachment's function by decreasing the structure's ability to absorb mechanical stress before failure and cause for increased stress concentrations, which reduces the structure's ability to resist failure (Deymier et al., 2019). While anatomical studies in fish have described tendon-bone attachments at the macroscopic level, little emphasis has been placed on how tendon and bone connect at the microscopic level (Rønning et al., 2017).

Moreover, it is unknown whether or not these attachments are capable of responding to novel force regimes by undergoing remodeling, which could influence how they function.

In fish, undulatory locomotion is achieved by the sequential and wavelike contraction of muscle segments (myomeres), which are tightly nested within one another along the length of a fish's body. A contiguous network of connective tissues (skin and septa) surrounding the myomeres is suggested to be responsible for the transfer of muscular forces to the backbone of fish (S. Gemballa et al., 2003; J. H. Long et al., 2002; J. Long et al., 1996; Westneat et al., 1993; Westneat & Wainwright, 2001). Separating the dorsal epaxial muscle from the ventral hypaxial muscle in fish is the horizontal septum, which connects the fish's backbone, to its skin (Westneat et al., 1993; Westneat & Wainwright, 2001). Embedded within the horizontal septum of most species of fish are epicentral tendons. Each tendon attaches medially to the centrum of a vertebra, and projects laterally towards the fish's skin (Westneat et al., 1993; Westneat & Wainwright, 2001). The angle that epicentral tendons make with respect to each centrum increases as you approach the tail of the fish (Westneat et al., 1993; Westneat & Wainwright, 2001). It has been proposed that the epicentral tendons experience tension when the epaxial and hypaxial muscles—in between which they are wedged—contract and expand radially, and that they are likely involved in force transfer during swimming (Westneat et al., 1993).

Based on the knowledge we have about how tendon, bone, and tendon-bone attachments undergo remodeling in response to novel force regimes, we hypothesized that unloading of the epicentral tendon-vertebra attachment would alter its force environment, resulting in its remodeling. We tested this hypothesis by severing a subset of epicentral tendons at their distal ends in rainbow trout. We assessed the effect of localized unloading on tendon attachments for the severed tendons, as well as their ipsilateral and contralateral neighbors. Bone percentage and cellular density were quantified across the attachment using histology and the material properties of the attachment were quantified using tensile-testing. First, we predicted that unloaded attachments would alter their cellularity and extracellular matrix content and organization, resulting in altered material properties. Second, we predicted that loaded attachments from neighboring regions would alter their mechanical behavior to compensate for the unloading of a subset of attachments, as well as their cellularity, extracellular matrix content and organization, and material properties. In this chapter, we present and discuss the material properties testing findings.

3.2 | MATERIALS AND METHODS

The study took place at the University of Ottawa, between September 2018 and March 2020. All fish were obtained from Linwood Acres Trout Farm (Campbellcroft, ON, Canada) and were housed in the University of Ottawa's aquatic facility. Fish surgical severing and euthanization was conducted according to University of Ottawa ACVS protocol BL-1926.

Surgical Severing of the Epicentral Tendons in Experimental Fish

Thirty-six *Oncorhynchus mykiss* (length 32.6 ± 0.3 cm, weight 445.1 ± 11.0 g) were anesthetized using a 100mg/L solution of MS-222 (tricaine methanesulfonate) buffered with sodium bicarbonate. Average surgery duration (time into MS-222, to time recovered) ranged between 3 and 11 minutes (6.1 ± 0.3). Water was pumped over the gills during surgery. A sterilized scalpel was used to make an approximate 75° angle (downward) incision (~1 cm in length) with respect to the frontal plane, above the horizontal septum and within the dorsal-adipose region (Fig. 3.1). Upon crossing the horizontal septum, the scalpel was arced in the anterior direction to sever multiple epicentral tendons within the horizontal septum. A syringe was used to inject approximately 2 mL of water-based acrylic paint inside the incision to mark the incision and indicate which tendons had been cut, as well as prevent contact and possible healing between the severed ends of the tendons. Half of the fish were incised on their right side, and the other half on their left side. Fish were allowed to recover for 6 weeks and 2 days. To prevent fungus they were treated with 5ppt Instant Ocean® Sea Salt (Blacksburg, VA) for 5 days, and 2 doses of 10 mg/L Praziquantel, twice, 2 weeks apart. Three fish died during the recovery period, leaving a total of 33 fish.

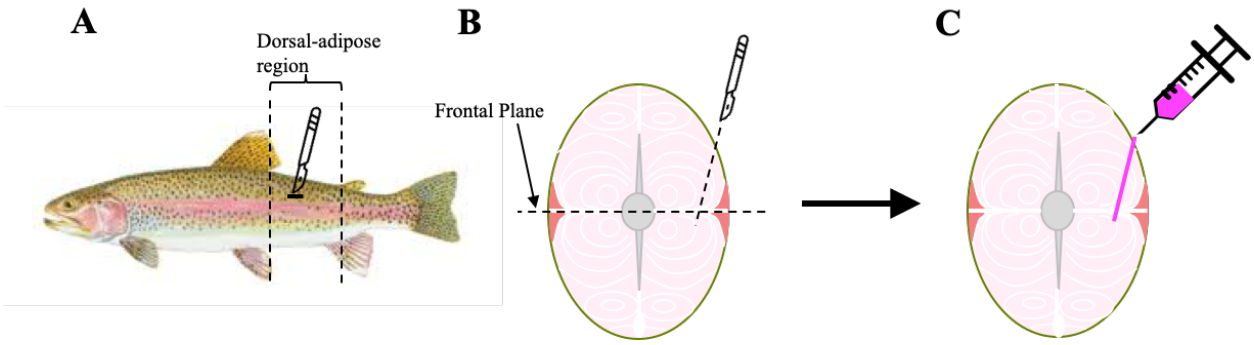

Fig. 3.1. Schematic illustrating how epicentral tendons within the dorsal-adipose tissue region were severed at their distal ends in anesthetized fish. **A**, the incision (~1 cm in length) was made within the dorsal-adipose region. Fish schematic obtained from "Happy Hooker Charters, Fishing Booker" (n.d.). Scalpel schematic obtained from "Online Wed Fonts: Scalpel Free Icon" (n.d.). **B**, a cross section of the dorsal-adipose region. A scalpel was inserted above the horizontal septum, on an approximate 75° angle with respect to the frontal plane. The surgical cut was made so that tendons were severed at their distal end, near the skin. Upon crossing the horizontal septum, the scalpel was arced in the anterior direction. Scalpel schematic obtained from "Online Wed Fonts: Scalpel Free Icon" (n.d.). **C**, the wound was filled with acrylic water-based paint to mark the incision as well as prevent contact between the severed ends of the tendons. Needle schematic modified from "Web Stock Review: Needle Clipart Medical" (n.d.).

Material Properties Testing of Attachments in Operated and Control Fish

Twenty-eight recovered rainbow trout (18 females, 10 males; length 32.5 ± 0.3 cm, weight 421.2 ± 12.8 g) were euthanized and the dorsal-adipose tissue segment was excised from each. Side of the fish on which the incision was made had no effect on material properties and therefore, data from both sides of the fish was pooled. Material properties of tendon attachments were quantified at the site of injury (region 5), anterior and posterior to the cut site on both sides of the fish (regions 1, 3, 4, 6), and on the uncut tendon opposite the injury site (region 2) (see Fig. 3.2 for numeric values assigned to tendon attachments from these regions). Due to the method of extracting tendons for material properties testing, only attachments from one side of the fish could be extracted; attachments were extracted from the cut side of 14 operated fish, and the uncut side of 14 operated fish.

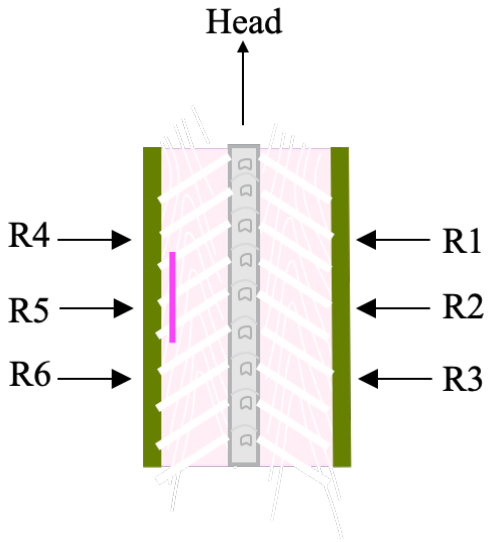

Fig. 3.2. Schematic illustrating the numeric values assigned to the different regions from which tendon attachments were extracted for tensile-testing within operated fish. Regardless of the side of the fish that was surgically cut, attachments from region 1 (R1) were always anterior to, and opposite the cut; attachments from region 2 (R2) were always directly opposite the cut; attachments from region 3 (R3) were always posterior to, and opposite the cut; attachments from region 4 (R4) were always anterior to the cut; attachments from region 5 (R5) were always within the cut; attachments from region 6 (R6) were always posterior of the cut. Note that the head of the fish is found above the schematic, while the tail of the fish is found below the schematic.

Tendon to bone attachment position within the dorsal-adipose tissue segment was recorded for each excised attachment, then samples were placed in 1X tris-buffered saline prior to tensile-testing. Tensile-testing and data transformations were conducted according to previously described methods in Chapter 2. All attachments were tensile-tested with the tendons positioned on a 45° angle with respect to the long axis of the vertebrae. Trials were kept if the tendon was long enough to be grabbed by the bottom gripper and if the tendon did not slip through the gripper during tensile-testing. In addition, successful severing of the tendon(s) was required in order to keep all trials from a fish (as evidenced by a visible interruption with or without paint at the tendon incision site) (Fig. 3.3). A group of 5 control fish (1 female, 4 males; length 35.1 ± 0.6 cm, weight 529.0 ± 36.6 g) that did not undergo surgical intervention were also

tested for comparison. Attachments for these controls were sampled using the same protocol as described for tensile-testing in Chapter 2. Going forward we will always refer to the fish that have not undergone surgery as “control” and those that have undergone surgery as “operated” fish.

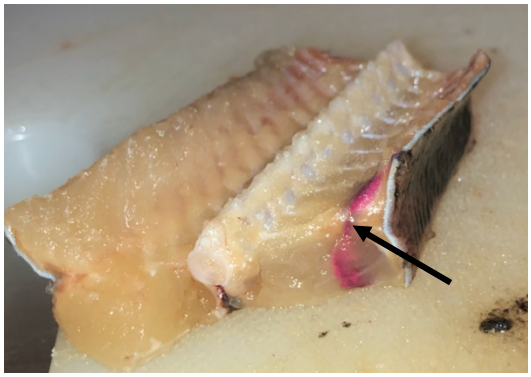

Fig. 3.3. An example of a post-recovery fish in which the operation successfully severed an epicentral tendon at its distal end. The arrow indicates the visible interruption of a tendon at the incision site.

Histological Preparation of Specimens in Operated and Control Fish

Attachment samples were divided into four groups for histological analysis: 1) unpulled attachments from control fish (3 females, 1 male; length 33.8 ± 0.5 cm, weight 447.0 ± 20.9 g), 2) pulled attachments from control fish (1 female, 4 males; length 35.1 ± 0.6 cm, weight 529.0 ± 36.6 g), 3) unpulled attachments from operated fish (1 female, 4 males; length 33.3 ± 0.7 cm, weight 450.5 ± 12.5 g), and 4) pulled attachments from operated fish (18 females, 10 males; length 32.5 ± 0.3 cm, weight 421.2 ± 12.8 g).

Control and operated unpulled samples were fixed in 10% buffered formalin for 7 days at room temperature. Control and operated pulled samples were fixed in 10% buffered formalin for 3 days (2 days at room temperature, 1 day at 4 °C). All samples were decalcified in 12.5% formic acid for 3 days at 4 °C. All samples underwent paraffinization at the University of Ottawa’s Histology Core Facility.

Statistical Analyses

Linear mixed effects modeling and Bonferroni *post hoc* analyses in RStudio v1.2.5019 were conducted for all statistical analyses. Models contained the fixed effects of interest, regardless of their significance. Additional fixed effects (weight, length, sex, side of the fish) were included in models when statistically significant (as determined by both model comparison and in the final model itself). See tables 3.1 and 3.3 for summaries of models used. *p* values of less than 0.05 were considered statistically significant. All values were presented as means ± standard error of the means. Estimated marginal means are presented for the linear mixed effects models. Linear modelling and Bonferroni *post hoc* analyses were conducted to determine which groups of attachments did not differ in their average tendon attachment position within the dorsal adipose tissue segment ($p > 0.05$) (model: Tendon Position ~ Group).

Contributions of Other Authors: Cassandra Donatelli conducted material properties testing on attachments isolated by Emily MacMaster and applied data transformations.

3.3 | RESULTS

Location of Failure

During tensile-testing, the location of failure always occurred within the tendon and never in the bone.

Comparing Uncut Attachments to Cut Attachments

Average tendon attachment position did not differ between uncut attachments from unoperated control fish and cut attachments (R5) from operated fish ($p > 0.05$). Therefore, any differences in material properties between these groups can be explained by the surgical intervention and not due to the fact that average tendon attachment position differs between the compared groups.

There was no significant difference in mean maximum load and mean maximum extension between uncut attachments from unoperated control fish and cut attachments (R5) from operated fish ($p > 0.05$) (Tables 3.1–3.2; Fig. 3.4A, B).

Table 3.1. Model summary and ANOVA results for linear mixed effects models used in the analyses comparing the material properties of uncut attachments from unoperated control fish and cut attachments from operated fish. $\alpha = 0.05$. The p-values of significant predictors ($p < 0.05$) are in bold.

Analysis	Material Properties Testing				Material Properties Testing			
Model: Response Variable Random Effects	Maximum Load Fish				Maximum Extension Fish			
	num DF	den DF	F	*P*	num DF	den DF	F	*P*
Fixed Effects:								
Group (Uncut Tendon Attachments/Cut Tendon Attachments)	1	15	0.06	0.8151	1	15	0.75	0.4015

Table 3.2. Estimated marginal means ± standard errors of maximum loads and maximum extensions as a function of group. Estimated marginal means ± SE were calculated using the linear mixed effects models used in the analyses comparing the material properties of uncut attachments from unoperated control fish and cut attachments from operated fish (Table 3.1).

Group	Maximum Load (N)	Maximum Extension (mm)
Uncut Tendon Attachments	1.49 ± 0.2	1.03 ± 0.3
Cut Tendon Attachments	1.55 ± 0.1	1.37 ± 0.2

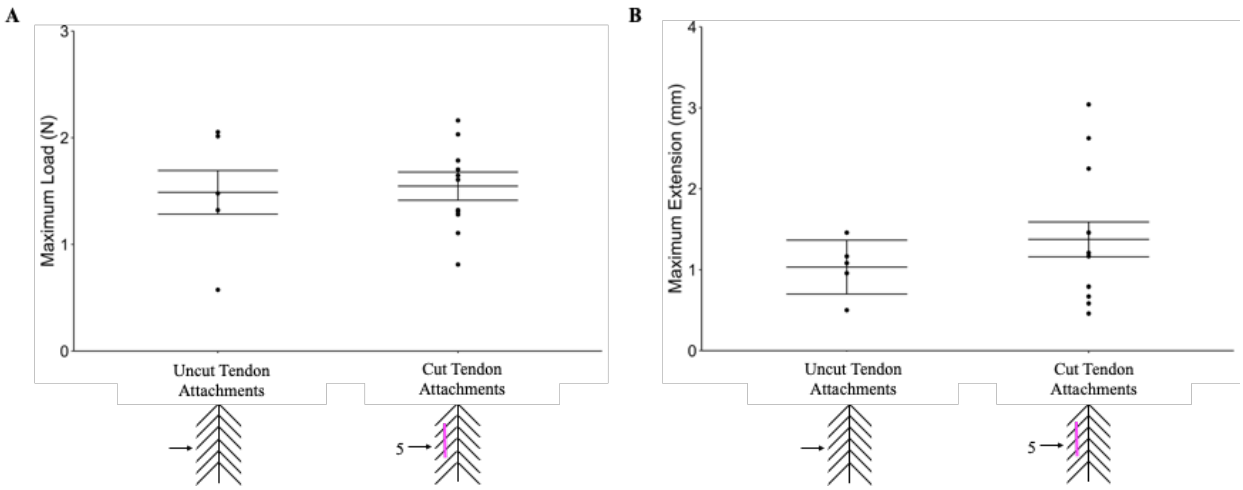

Fig. 3.4. Mean maximum loads (N) and mean maximum extensions (mm) of uncut attachments from unoperated control fish and cut attachments from operated fish. All attachments were tensile-tested on 45° angles with respect to the vertebrae. Only data for tendon attachments originating from positions 4 and 6 were used for uncut tendon attachments, as they were found within the range of tendon attachment positions tested for cut tendon attachments. Estimated marginal means ± SE are presented. $\alpha = 0.05$. There was no significant difference in maximum load and maximum extension between uncut and cut attachments ($p > 0.05$, ANOVA for linear mixed effects model).

Comparing Attachments of Different Regions Within Operated Fish

Average tendon attachment position did not differ between attachments from regions directly across from one another (R1 vs. R4, R2 vs. R5, R3 vs. R6) ($p > 0.05$ for each comparison).

In a comparison of left and right side attachments, there was no significant difference in mean maximum load and mean maximum extension between attachments from regions directly opposite one another in operated fish (R1 vs. R4; R2 vs. R5; R3 vs. R6) ($p > 0.05$ for each comparison) (Fig. 3.5A, B). The mean maximum extension of attachments within operated fish generally decreased in the rostral-caudal direction (R3 < R1&R4 and R6 < R4, $p < 0.05$; Tables 3.3–3.4, Fig. 3.5B). The mean maximum load of attachments from region R3 was significantly

lower than that of attachments from region R5 in operated fish ($p < 0.05$) (Tables 3.3–3.4; Fig. 3.5A).

Overall, mean maximum load increased with increasing fish total body length ($p < 0.05$) (Table 3.3; Fig. 3.5A).

Table 3.3. Model summary and ANOVA results for linear mixed effects models used in the analysis comparing the material properties of attachments from different regions (R1, R2, R3, R4, R5, R6) within operated fish. $\alpha = 0.05$. The p values of significant predictors ($p < 0.05$) are in bold.

Analysis	Material Properties Testing				Material Properties Testing			
Model: Response Variable Random Effects	Maximum Load Fish				Maximum Extension Fish			
	num DF	den DF	F	*P*	num DF	den DF	F	*P*
Fixed Effects†:								
Tendon Attachment Region in Operated Fish (R1-6)	5	44	2.72	**0.0315**	5	44	5.81	**0.0003**
Fish TBL	1	24	9.40	**0.0053**	-	-	-	-

† In model comparisons, fish total body length (TBL) was a significant predictor of mean maximum load and therefore was included in the model.

Table 3.4. Estimated marginal means ± standard errors of maximum loads and maximum extensions as a function of tendon attachment region within operated fish. Estimated marginal means ± SE were calculated using the linear mixed effects models used in the analysis comparing the material properties of attachments from different regions (R1-6) within operated fish (Table 3.3).

Tendon Attachment Region Within Operated Fish	Maximum Load (N)	Maximum Extension (mm)
R1	1.4 ± 0.1	1.4 ± 0.2
R2	1.4 ± 0.1	1.2 ± 0.2
R3	1.1 ± 0.1	0.8 ± 0.2
R4	1.5 ± 0.1	1.6 ± 0.2
R5	1.5 ± 0.1	1.4 ± 0.2
R6	1.5 ± 0.1	0.8 ± 0.2

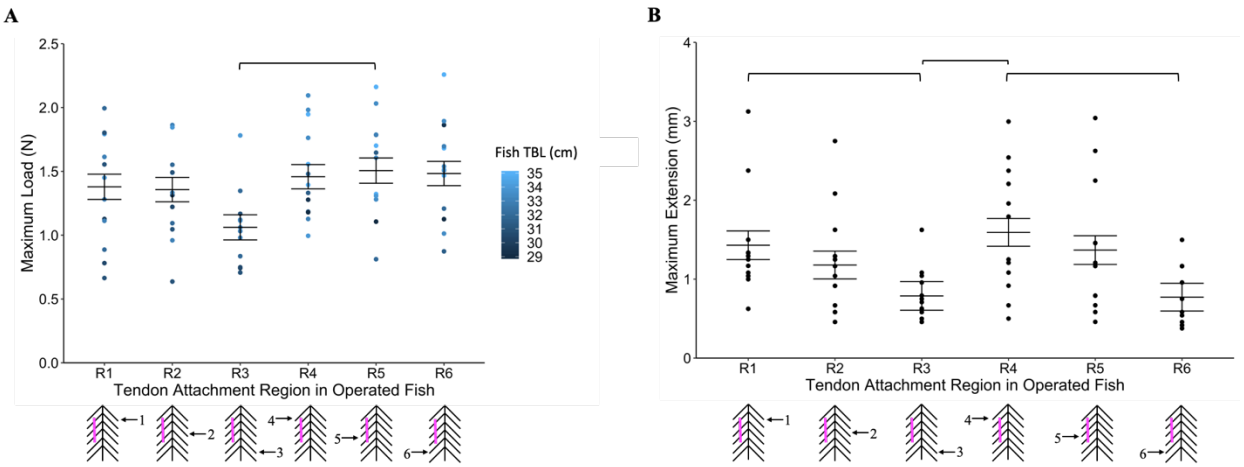

Fig. 3.5. Mean maximum loads (N) and mean maximum extensions (mm) of attachments originating from different regions (R1-6) within operated fish. All attachments were tensile-tested on 45° angles with respect to the vertebrae. Fish total body length (TBL) was a significant predictor of attachment maximum load (see gradient legend). Estimated marginal means ± SE are presented. $\alpha = 0.05$. Brackets denote significant differences in mean maximum load and mean maximum extension between tendon attachment regions ($p < 0.05$, Bonferroni *post hoc).*

3.4 | DISCUSSION

Tendon Unloading Does Not Alter Attachment Material Properties

Contrary to what was predicted, the severing of the epicentral tendons at their distal ends and consequential unloading of the tendon-bone attachments had no effect on the material properties of the attachments. This finding suggests that either no modifications of structure and/or composition of the attachment took place following their severing, or that any modifications that may have occurred, were not enough to sufficiently alter the material properties of the attachment.

The material properties of tendon, such as maximum load, have been shown to be significantly lower within rabbit tendons subjected to unloading for 3 weeks (Loitz et al., 1989). Furthermore, tendon-bone attachments in mice have undergone alterations in structure and material properties in 3 weeks (Deymier et al., 2019). The amount of time required to observe

changes in the structure, composition, and material properties of fish tendon-bone attachments in response to novel force regimes has yet to be elucidated. However, fish bone has been shown to undergo remodeling in 5 weeks in response to changes in mechanical loading (Du & Standen, 2020). As a result, we would expect that the time we allowed for tissue remodeling (6 weeks, 2 days) was sufficient to result in modifications to the attachment's structure and/or composition and therefore, to its material properties.

There are several possible explanations for why no differences in material properties were observed following unloading. First, severing of the attachments at their distal end may not have resulted in sufficient unloading of the attachments to cause for modifications in structure and/or composition and altered material properties. The epicentral tendons are part of a contiguous network of connective tissues that experience tension in response to radially-expanding muscle. As the epicentral tendons are embedded within the horizontal septum—whose connections to the surrounding muscle, skin, and vertebrae were maintained following surgical intervention—it is possible that tendons may have continued to experience tension as part of the intact horizontal septum. Moreover, the epicentral tendons are tightly wedged in between the epaxial and hypaxial muscle, which may have supported the maintenance of their function. Alternatively, it is possible that remodeling did take place, but that the resulting differences in material properties were too small to be detected by our methodology. In this case, the use of a tensile-testing apparatus with a higher resolution could be implemented. It is also possible that operations may have had greater effects on other tissues. For example, fish may have spent energy in the healing of damaged muscular tissue.

The Effect of Localized Unloading on Intact Attachments From Neighboring Regions

Contrary to what was predicted, there was no significant difference in material properties between attachments from regions directly opposite one another within operated fish, which suggests that attachments on the unoperated side did not alter their mechanical behavior to compensate (i.e. no limping effect) for the unloading of attachments on the operated side. If attachments whose tendons were severed were not successfully unloaded as described above, it would make sense that the force environment of contralateral attachments remained unchanged.

In comparing the material properties of tendon attachments found in different positions within the dorsal-adipose tissue segment in Chapter 2, we observed that tendon attachments had

higher mean maximum loads and lower maximum extension values at the nose compared with the tail (Chapter 2, Tables 2.5–2.6; Fig. 2.7A, B). In this experiment, mean maximum loads of attachments did not change towards the tail and maximum extension actually decreased towards the tail. Differences in rostral-caudal trends in material properties may be due to the injury inflicted during surgery, which could have altered swimming mechanics in the rostral-caudal direction (i.e. body wave amplitude), affecting the magnitude of forces experienced by attachments, which could have had an effect on attachment structure, composition, and material properties along the rostral-caudal direction.

3.5 | CONCLUSION

We studied the effect of unloading on the material properties of the epicentral tendon-vertebra attachment in rainbow trout. Severing of epicentral tendons at their distal end had no effect on attachment material properties. It is likely that the network of connective tissues in which the epicentral tendons are embedded, as well as the epaxial and hypaxial muscle in between which tendons are wedged, may have supported the maintenance of their function in transferring force to the backbone. In this way, the anatomy of the connective tissue continuum and nested muscle myomeres may confer flexibility to the fish's musculoskeletal system, in that it enables proper biomechanical functioning despite local injury.

CHAPTER 4.

Discussion

4.1 | DISCUSSION

Statement of Purpose

In tendinous attachments of the vertebrate musculoskeletal system, forces generated by contracting muscles are transmitted to the bone, via the tendon, across muscle-tendon and tendon-bone interfaces. As tendon and bone differ vastly in their structure, composition, and material properties—such as stiffness—force transfer across tendon-bone interfaces can lead to the generation of stress concentrations at these interfaces. These stress concentrations can increase the risk of attachment failure.

Studies of the microstructure of fibrocartilaginous tendon-bone attachments in mammals have shed light on the role they play in mediating efficient force transfer between tendon and bone, while dissipating mechanical stresses at the interface, to minimize the risk of attachment failure. Studies have also shed light on the importance of mechanical stimulation in maintaining the structure of tendon-bone attachments so that they may maintain proper functioning. Unloading of tendon-bone attachments has caused adverse remodeling of attachment structure and caused compromised mechanics.

In fish, contractile forces generated by muscles are transferred to the backbone via a contiguous network of tendinous connective tissue septa, which causes it to bend in a wavelike manner. The macroscopic anatomy of the connective tissue network has been described extensively, however, little is known about how these connective tissues attach to the bone at the microscopic level to accomplish force transfer. Furthermore, the ability these tendon-bone attachments to undergo remodeling in response to changes in the degree of mechanical loading, which could impact their function, remains to be elucidated. In this study, we shed light on the epicentral tendon-vertebra attachment by characterizing its microstructure and material properties. In addition, we studied the effect of unloading on the attachment's material properties.

Interpretation of Key Findings and Future Directions

Tendon Angle

In a rainbow trout at rest, the angle of the epicentral tendons with the vertebral centrum increases as you move towards the tail. The same finding has been reported for scombrid fishes

(Westneat et al., 1993). Whether or not epicentral tendon angle changes when a fish is swimming, is unknown. In Chapter 2, we propose that the increase in epicentral tendon angle towards the tail of the resting fish may be related to the increase in body wave amplitude that the fish experiences towards its tail when it is swimming. The increase in body wave amplitude towards the tail of the fish may cause tendons towards the posterior to become stretched, decreasing the angle that they make the vertebral centra. Therefore, although posterior tendons have larger angles that more closely resemble 90° when the fish is at rest, the angle along which they actively transfer force to the backbone during swimming may more closely resemble 45°.

Although changes in epicentral tendon angle may occur within a swimming fish, we also predict that the anatomy of the fish would ultimately limit the angle change that epicentral tendons could experience during undulatory locomotion. Histological analyses of the epicentral tendon-vertebra attachment revealed that attachments lack fibrocartilage. The amount of fibrocartilage present at tendon-bone attachment is positively correlated with the amount of angle change that the respective tendon experiences relative to the bone, during force transmission (Benjamin & Ralphs, 1998). As the epicentral tendon-vertebra attachment lacks fibrocartilage, we would predict that the epicentral tendons do not experience large changes in angle with respect to the bone during force transmission. Moreover, material properties testing of attachments along the length of the fish revealed that attachments performed differently when tensile-tested on different angles, further supporting the notion that epicentral tendons are optimized to transfer force along particular angles, as opposed to a large range of angles. The dynamic modeling of epicentral tendons within the dorsal-adipose tissue segment of a swimming fish would allow us to determine if the epicentral tendons change angle with the bone during swimming and the extent of any angle change.

The Epicentral Tendon-Vertebra Attachment is a Fibrous Attachment

Individual collagen fibers of the epicentral tendon projected directly into a layer of cancellous vertebral bone, which surrounded a layer of cortical bone. Previous descriptions of tendon-bone attachments have described tendons as inserting into a thin layer of cortical bone, which surrounds cancellous bone. The functional implications of these differing bone structures at the tendon-bone attachment site have yet to be studied.

The epicentral tendon's collagen fibers projected into the bone on the same angle that the tendon made with the bone and continuations of the tendon's fibers were visible within the bone. We identified these continuations as being Sharpey's fibers. Traditionally described as serving as anchors for tendons, periosteum, and ligaments to bone, Sharpey's fibers may also confer flexibility and extensibility to tendon-bone attachments, owing to coils of elastin have been found to surround individual Sharpey's fibers (Aaron, 2012). In future studies, it would be interesting to analyze the composition of the Sharpey's fibers within the bone of the epicentral tendon-vertebra attachment as they may contribute to the material properties of the attachment, such as its extensibility.

The tendon in proximity to the interface was densely populated with cells possessing rounded nuclei. The tendon distal to the interface was less densely populated with cells possessing nuclei with an elongate morphology. The cells within the tendon have yet to be identified. I predict that both cell types correspond to tenocytes. However, I predict that the relative metabolic activities of these tenocytes differs, since round tenocytes have been shown to exhibit increased secretion of tendon extracellular matrix precursors (Huisman et al., 2014). To test the hypothesis that both cell types correspond to tenocytes, I could conduct immunohistochemistry. Both *Scleraxis* and *Tenomodulin* are tendon-specific biomarkers of tenocytes (Thankam et al., 2018). In the event that both cell types correspond to tenocytes, I can test the hypothesis that their relative metabolic activities differ by using immunohistochemistry to compare their expression levels of extracellular matrix collagen precursors, such as pro-collagen I (Sai Chuen et al., 2004).

The implementation of other imaging techniques could provide a more complete picture of the epicentral tendon-vertebra attachment. Histological sections provided a 2-dimensional (2D) representation of the epicentral tendon-vertebra attachment. A complete 3-dimensional picture (3D) of the attachment could be obtained by scanning serial sections and stacking them to create a 3D rendering (z-stacking), or by using micro computed tomography to scan the attachment (Rossetti et al., 2017). A 3D rendering of the tendon's footprint on the bone would provide a more complete picture of the attachment surface area, which we determined to be sinuous using 2D histological sections. Furthermore, a more complete picture of bone structure and cellularity in the region of the attachment site and in regions surrounding the attachment site could be obtained using 3D imaging techniques. Imaging attachments at a higher resolution

(confocal or electron microscopy) and magnification (electron microscopy) could allow for the detection of microstructures that may have not been visible using brightfield light microscopy. For instance, Rosetti et al. (2017) characterized the fibrocartilaginous Achilles tendon-bone attachment using confocal microscopy and scanning electron microscopy and found that tendon collagen fibers unravelled and splayed prior to their insertion into the bone, allowing for a broadened tendon attachment on the bone (Rossetti et al., 2017). Whether or not the epicentral tendon's collagen fibers unravel at the interface, remains unknown.

Rostral-Caudal Trends in Attachment Material Properties

Differences in attachment material properties at different positions along the length of the fish suggest that attachments differ in their structure and/or composition depending on their position along the backbone. Differences in attachment structure and/or composition may be reflective of relative force environments the attachments are found in. Attachments towards the head of the fish may experience larger forces due to their association with larger myomeres capable of producing larger forces, whereas attachments towards the tail of the fish may experience smaller forces due to their association with smaller myomeres, which produce smaller forces. As a result, attachments towards the head of the fish may be required to possess a structure and/or composition that confers them with higher tensile strength (such as higher collagen content, or larger tendon cross-sectional area), in comparison to attachments towards the tail of the fish. The histological analysis of attachments found at different positions along the length of the fish would provide insight into any differences in attachment structure and/or composition. As a specific example, histological cross sections of tendons at different positions within the dorsal adipose tissue segment within a subset of fish could be obtained.

Interestingly, the rostral-caudal trends in attachment material properties observed for operated fish from Chapter 3, differed from those observed in unoperated fish from Chapter 2. In Chapter 3, we propose that the injury inflicted by the cut may have altered the fish's swimming mechanics along the rostral-caudal direction (such as altered body wave amplitude), which may have led to changes in attachment structure and/or composition towards the posterior of the fish. Changes in rostral-caudal swimming mechanics due to surgery could be detected by comparing the swimming mechanics of an unoperated and operated fish.

Unloading Had No Effect on Attachment Material Properties

Severing of epicentral tendons had no effect on attachment material properties. As the material properties of a material depend on its structure and composition, this finding suggests that either no alterations in structure and/or composition took place in response to unloading, or that any modifications that may have taken place, were not significant enough to alter the material properties of the attachment. To confirm whether or not attachments altered their structure and/or composition in response to unloading, samples from Chapter 3 can be analyzed histologically using the techniques employed in Chapter 2. We predict that unloaded attachments would alter their bone structure and cellularity adjacent to the interface. Unloading of vertebrate bone has been shown to result in the apoptosis of osteocytes (Aguirre et al., 2006) and increased bone resorption (Friedman et al., 2019; Lang et al., 2004; Leblanc et al., 2000). Unloading of tendon-bone attachments has also been shown to result in bone loss at the interface (Deymier et al., 2019). As a result, we predict that bone percentage and osteocyte density in proximity to the interface would decrease in response to unloading of the attachment. If the high density of rounded cells within the tendon in proximity to the interface correspond to tenocytes responding to mechanical stimulation (determined using antibodies for scleraxis, tenomodulin, and pro-collagen precursors), we predict that they would become less densely populated, less rounded, and less metabolically active in response to unloading of the attachment. Additional quantitative analyses could be carried out to detect changes in attachment structure and/or composition, such as measurements of collagen fiber alignment (shown to decrease in response to unloading [Bayer et al., 2014]), measurements of tendon footprint surface area (2D as per our methods, or 3D using by stacking scanned sections or microcomputed tomography [Zumwalt, 2006]), and measurements of Sharpey fiber diameter and density using scanning electron microscopy (J. E. Anderson et al., 1993). Furthermore, a proteomic analysis could be carried out to detect small changes in attachment protein content and quantity (such as collagen) (Turko et al., 2017).

Challenges Associated with Studying the Epicentral Tendon-Vertebra Attachment as Part of a Contiguous Network of Connective Tissues

Owing to the complexity of the tendinous connective tissue sheet network found within fish, it is difficult to gain insight into the functioning of the network as a whole in transferring force to the backbone using material properties testing. Consequently, we must resort to studying

individual components of the network, which has its limitations. For instance, as individual epicentral tendon-vertebra attachments were extracted from their natural *in vivo* environment to allow for tensile-testing, the epicentral tendon's interactions with the contiguous network of connective tissues were removed. As a result, this limits the extrapolations that can be made regarding the functioning of these epicentral tendons within their natural *in vivo* environment.

In the event that severing of attachments had no effect on the structure, composition, and material properties of the attachment, it is likely that attachments were not successfully unloaded due to the epicentral tendons' connections to a larger network of interconnected tissues (muscle, septa, skin and bone). The fusion of all of the fish's musculoskeletal parts minimizes the chance of failure of any one part and means that major muscle injury can be overcome as the function of the whole system does not fail. Consequently, unloading of a single epicentral tendon-vertebra attachment within the system may prove to be difficult.

An alternative approach to studying the effect of changing load regime on epicentral tendon-vertebra attachment structure, composition, and material properties would be to subject the entire network of connective tissues within the fish's musculoskeletal system to increased loading in a controlled swimming experiment. In this type of experiment, fish would be forced to swim against a current. These types of experiments have been shown to result in increased bone mineral density and increased osteocyte density within the vertebra of fish (Totland et al., 2011). An added benefit to this type of experiment is that it is non-invasive, meaning that a fish's energy would be spent on remodeling and not on wound-healing.

CONCLUSION

We characterized the microstructure and quantified the material properties of the epicentral tendon-vertebra attachment in rainbow trout and studied the effect of unloading on the attachment's material properties.

We classified the epicentral tendon-vertebra attachment as being a fibrous attachment. The presence of numerous fibrous epicentral tendon-vertebra attachments along the length of the backbone suggests that rainbow trout may serve as an excellent model for studying this unusual type of tendon-bone attachment, of which little is known outside of its general structure. To our knowledge this is the first study to describe the microstructure of a tendon insertion into cancellous bone which lacks a bone cortex. Cellularity within the tendon was not uniform; cells within the tendon at the interface appeared more rounded and were densely populated, whereas cells within the tendon distal to the interface appeared more elongate and were less densely populated. It would be expected that tissues at the tendon-bone interface experience a greater degree of mechanical stimulation, as mechanical stresses tend to concentrate at tendon-bone interfaces. Therefore, we predict that the cells within the tendon adjacent to the interface correspond to tenocytes responding to mechanical stimulation, as tenocytes have been shown to respond to mechanical stimulation by increasing in number and becoming more rounded. Immunohistochemistry could be used to confirm the identities of the cells proximal and distal to the interface as well as compare their metabolic activities.

In resting fish, epicentral tendons increased in angle with the backbone towards the tail. While epicentral tendons may change angle with the backbone when the fish is swimming, we predict that tendons are not optimized to experience large changes in angle as evidenced by the absence of fibrocartilage at the tendon-bone attachment site and the finding that attachments exhibited different material properties when tensile-tested on different angles. Dynamic modeling of epicentral tendons within a swimming fish would provide insight into the angles along which epicentral tendons impart force onto the bone.

Severing of epicentral tendons had no effect on attachment material properties, which suggests that attachments did not undergo alterations in their structure and/or composition. This can be confirmed by conducting a histological analysis of attachments. We predict that the contiguous network of connective tissues in which the epicentral tendons are embedded and the surrounding musculature supported their maintenance of function. A controlled swimming

experiment in which all of the fish's musculoskeletal parts are subjected to increased loading may be a suitable alternative in studying the effect of changing load regime on attachment structure, composition, and material properties.

Future studies could characterize the epicentral tendon-vertebra attachment at a higher resolution and magnification, and using 3D techniques so that we may gain a better understanding as to how this attachment functions in mediating efficient force transfer from tendon, to bone—two materials which differ vastly in their structure, composition, and material properties.

BIBLIOGRAPHY

Aaron, J. E. (2012). Periosteal Sharpey's fibers: a novel bone matrix regulatory system? *Frontiers in Endocrinology*, *3*, 98.

Abraham, T., Fong, G., & Scott, A. (2011). Second harmonic generation analysis of early Achilles tendinosis in response to in vivo mechanical loading. *BMC Musculoskeletal Disorders*, *12*, 26.

Aguirre, J. I., Plotkin, L. I., Stewart, S. A., Weinstein, R. S., Parfitt, A. M., Manolagas, S. C., & Bellido, T. (2006). Osteocyte Apoptosis Is Induced by Weightlessness in Mice and Precedes Osteoclast Recruitment and Bone Loss. *Journal of Bone and Mineral Research*, *21*, 605–615.

Alexander, N. (1969). The Orientation of Muscle Fibres in the Myomeres of Fishes. *Journal of the Marine Biological Association of the United Kingdom*, *49*, 263–290.

Altringham, J. D., & Ellerby, D. J. (1999). Fish swimming: patterns in muscle function. *Journal of Experimental Biology*, *202*, 3397–3403.

Anderson, J. E., Lentz', D. L., Johnson, R. B., & Anderson, J. E. (1993). Recovery from Disuse Osteopenia Coincident to Restoration of Muscle Strength in mdx Mice. *Bone*, *14*, 625–634.

Anderson, K. (2019). Tendon to Bone Reattachment Surgery: Understanding the Procedure. Retrieved August 6, 2020, from https://mend.me/tendon-to-bone-reattachment-surgery-understanding-your-sports-medicine-procedure/

Andersson, G., Forsgren, S., Scott, A., Gaida, J. E., Stjernfeldt, J. E., Lorentzon, R., … Danielson, P. (2011). Tenocyte hypercellularity and vascular proliferation in a rabbit model of tendinopathy: contralateral effects suggest the involvement of central neuronal mechanisms. *British Journal of Sports Medicine*, *45*, 399–406.

Apostolakos, J., Durant, T. J., Dwyer, C. R., Russell, R. P., Weinreb, J. H., Alaee, F., … Mazzocca, A. D. (2014). The enthesis: a review of the tendon-to-bone insertion. *Muscles, Ligaments and Tendons Journal*, *4*, 333–342.

Arampatzis, A., Peper, A., Bierbaum, S., & Albracht, K. (2010). Plasticity of human Achilles tendon mechanical and morphological properties in response to cyclic strain. *Journal of Biomechanics*, *43*, 3073–3079.

Atkins, A., Milgram, J., Weiner, S., & Shahar, R. (2015). The response of anosteocytic bone to

controlled loading. *Journal of Experimental Biology*, *218*, 3559–3569.

Barton, J. M., & Keenan, R. M. (1967). The formation of Sharpey's fibres in the hamster under nonfunctionla conditions. *Archives of Oral Biology*, *12*, 1331–1336.

Bayer, M. L., Schjerling, P., Herchenhan, A., Zeltz, C., & Heinemeier, K. M. (2014). Release of Tensile Strain on Engineered Human Tendon Tissue Disturbs Cell Adhesions, Changes Matrix Architecture, and Induces an Inflammatory Phenotype. *PLOS ONE*, *9*, e86078.

Benjamin, M., Evans, E. J., & Copp, L. (1986). The histology of tendon attachments to bone in man. *Journal of Anatomy*, *149*, 89–100.

Benjamin, M., Kumai, T., Milz, S., Boszczyk, B. ., Boszczyk, A. ., & Ralphs, J. . (2002). The skeletal attachment of tendons—tendon 'entheses.' *Comparative Biochemistry and Physiology Part A: Molecular & Integrative Physiology*, *133*, 931–945.

Benjamin, M., & Ralphs, J. R. (1998). Fibrocartilage in tendons and ligaments - an adaptation to compressive load. *Journal of Anatomy*, *193*, 481–494.

Best, A., Holt, B., Troy, K., & Hamill, J. (2017). Trabecular bone in the calcaneus of runners. *PLOS ONE*, *12*, e0188200.

Bone, Q. (1972). Buoyancy and Hydrodynamic Functions of Integument in the Castor Oil Fish, Ruvettus pretiosus (Pisces: Gempylidae). *Copeia*, *1972*, 78–87.

Bricard, Y., Lebret, V., Lefevre, F., & Rescan, P.-Y. (2014). Early Fish Myoseptal Cells: Insights from the Trout and Relationships with Amniote Axial Tenocytes. *PLOS ONE*, *9*, e91876.

Buschmann, J., & Meier Bürgisser, G. (2017). Structure and function of tendon and ligament tissues. In *Biomechanics of Tendons and Ligaments* (pp. 3–29). Elsevier.

Cabahug, P. C. ;, Kennedy, O. D. ;, Laudier, D. M. ;, Majeska, R. J. ;, Khandelwal, S. ;, Judex, & Schaffler, M. B. +. (2012). *Unloading of mouse long bone causes widespread apoptosis of cortical osteocytes: spatial and temporal relationships to increased bone resorption*. Retrieved from http://www.ors.org/Transactions/58/0026.pdf

Chen, J.-H., Liu, C., You, L., & Simmons, C. A. (2010). Boning up on Wolff's Law: Mechanical regulation of the cells that make and maintain bone. *Journal of Biomechanics*, *43*, 108–118.

Chen, J. W., Galloway, J. L., Westerfield, M., Kimmel, C. B., Copeland, N. G., Gilbert, D. J., … Olson, E. N. (2014). The development of zebrafish tendon and ligament progenitors. *Development (Cambridge, England)*, *141*, 2035–2045.

Chicurel, M. E., Chen, C. S., & Ingber, D. E. (1998). Cellular control lies in the balance of forces. *Current Opinion in Cell Biology*, *10*, 232–239.

Currey, J. D. (2011). The Structure and Mechanics of Bone. *Journal of Materials Science*, *47*, 41–45.

De Boer, M. D., Selby, A., Atherton, P., Smith, K., Seynnes, O. R., Maganaris, C. N., … Rennie, M. J. (2007). The temporal responses of protein synthesis, gene expression and cell signalling in human quadriceps muscle and patellar tendon to disuse. *Journal of Physiology*, *585*, 241–251.

Dean, M. N., & Shahar, R. (2012). The structure-mechanics relationship and the response to load of the acellular bone of neoteleost fish: a review. *Journal of Applied Ichthyology*, *28*, 320–329.

Deymier-Black, A. C., Pasteris, J. D., Genin, G. M., & Thomopoulos, S. (2015). Allometry of the Tendon Enthesis: Mechanisms of Load Transfer Between Tendon and Bone. *Journal of Biomechanical Engineering*, *137*, 111005.

Deymier, A. C., Schwartz, A. G., Cai, Z., Daulton, T. L., Pasteris, J. D., Genin, G. M., & Thomopoulos, S. (2019). The multiscale structural and mechanical effects of mouse supraspinatus muscle unloading on the mature enthesis. *Acta Biomaterialia*, *83*, 302–313.

Du, T. Y., & Standen, E. M. (2020). Terrestrial acclimation and exercise lead to bone functional response in Polypterus senegalus pectoral fins. *Journal of Experimental Biology*, *223*, jeb217554.

Dwek, J. R. (2010). The periosteum: what is it, where is it, and what mimics it in its absence? *Skeletal Radiology*, *39*, 319–323.

Franchi, M., Fini, M., Quaranta, M., De Pasquale, V., Raspanti, M., Giavaresi, G., … Ruggeri, A. (2007). Crimp morphology in relaxed and stretched rat Achilles tendon. *Journal of Anatomy*, *210*, 1–7.

Friedman, M. A., Zhang, Y., Wayne, J. S., Farber, C. R., & Donahue, H. J. (2019). Single limb immobilization model for bone loss from unloading. *Journal of Biomechanics*, *83*, 181–189.

Fritton, J. C., Myers, E. R., Wright, T. M., & Van Der Meulen, M. C. H. (2005). Loading induces site-specific increases in mineral content assessed by microcomputed tomography of the mouse tibia. *Bone*, *36*, 1030–1038.

Gemballa, S, Hagen, K., Röder, K., Rolf, M., & Treiber, K. (2003). Structure and evolution of

the horizontal septum in vertebrates. *Journal of Evolutionary Biology*, *16*, 966–975.

Gemballa, Sven, Ebmeyer, L., Hagen, K., Hannich, T., Hoja, K., Rolf, M., … Weitbrecht, G. (2003). Evolutionary transformations of myoseptal tendons in gnathostomes. *Proceedings of the Royal Society B: Biological Sciences*, *270*, 1229–1235.

Gemballa, Sven, & Vogel, F. (2002). Spatial arrangement of white muscle fibers and myoseptal tendons in fishes. *Comparative Biochemistry and Physiology Part A: Molecular & Integrative Physiology*, *133*, 1013–1037.

Genin, G. M., Kent, A., Birman, V., Wopenka, B., Pasteris, J. D., Marquez, P. J., & Thomopoulos, S. (2009). Functional grading of mineral and collagen in the attachment of tendon to bone. *Biophysical Journal*, *97*, 976–985.

Gilotra, M. N., Shorofsky, M. J., Stein, J. A., & Murthi, A. M. (2016). Healing of rotator cuff tendons using botulinum toxin A and immobilization in a rat model. *BMC Musculoskeletal Disorders*, *17*, 127.

Gray, N.-M., Kainec, K., Madar, S., Tomko, L., & Wolfe, S. (2007). Sink or swim? Bone density as a mechanism for buoyancy control in early cetaceans. *The Anatomical Record: Advances in Integrative Anatomy and Evolutionary Biology*, *290*, 638–653.

Happy Hooker Charters, Fishing Booker. (n.d.). Retrieved from https://fishingbooker.com/charters/view/9861

Heinemeier, K. M., & Kjaer, M. (2011). In vivo investigation of tendon response to mechanical loading. *Journal of Musculoskeletal & Neuronal Interactions*, *11*, 115–123.

Herchenhan, A., Kalson, N. S., Holmes, D. F., Hill, P., Kadler, K. E., & Margetts, L. (2012). Tenocyte contraction induces crimp formation in tendon-like tissue. *Biomechanics and Modeling in Mechanobiology*, *11*, 449–459.

Hieronymus, T. L. (2006). Quantitative microanatomy of jaw muscle attachment in extant diapsids. *Journal of Morphology*, *267*, 954–967.

Huisman, E., Lu, A., Mccormack, R. G., & Scott, A. (2014). Enhanced collagen type I synthesis by human tenocytes subjected to periodic in vitro mechanical stimulation. *BMC Musculoskeletal Disorders*, *15*, 386.

Huysseune, A., Sire, J.-Y., & Meunier, F. J. (1994). Comparative study of lower pharyngeal jaw structure in two phenotypes of Astatoreochromis alluaudi (teleostei: Cichlidae). *Journal of Morphology*, *221*, 25–43.

Jayne, B. C., & Lauder, G. V. (1995). Are muscle fibres within fish myotomes activated synchronously? Patterns of recruitment within deep myomeric musculature during swimming in largemouth bass. *Journal of Experimental Biology*, *198*, 805–815.

Kastelic, J., Galeski, A., & Baer, E. (1978). The Multicomposite Structure of Tendon. *Connective Tissue Research*, *6*, 11–23.

Kjaer, M. (2004). Role of Extracellular Matrix in Adaptation of Tendon and Skeletal Muscle to Mechanical Loading. *Physiological Reviews*, *84*, 649–698.

Lang, T., LeBlanc, A., Evans, H., Lu, Y., Genant, H., & Yu, A. (2004). Cortical and Trabecular Bone Mineral Loss From the Spine and Hip in Long-Duration Spaceflight. *Journal of Bone and Mineral Research*, *19*, 1006–1012.

Leblanc, A., Schneider, V., Shackelford, L., West, S., Oganov, V., Bakulin, A., & Voronin, L. (2000). Bone mineral and lean tissue loss after long duration space flight. *Journal of Musculoskeletal and Neuronal Interactions*, *1*, 157–160.

Lee, D. D., & Glimcherl, M. J. (1991). Three-dimensional Spatial Relationship between the Collagen Fibrils and the Inorganic Calcium Phosphate Crystals of Pickerel (Americanus americanus) and Herring (Clupea harengus) Bone. *Journal of Molecular Biology*, *217*, 487–501.

Lee, R. F., Phleger, C. F., & Horn, M. H. (1975). Composition of oil in fish bones: possible function in neutral buoyancy. *Comparative Biochemistry and Physiology - B Comparative Biochemistry*, *50*, 13–16.

Liu, Y. X., Thomopoulos, S., Birman, V., Li, J.-S., & Genin, G. M. (2012). Bi-material attachment through a compliant interfacial system at the tendon-to-bone insertion site. *Mechanics of Materials*, *44*, 83–92.

Loitz, B. J., Zernicke, R. F., Vailas, A. C., & Kody, M. H. (1989). Effects of short-term immobilization versus continuous passive motion on the biomechanical and biochemical properties of the rabbit tendon. *Clinical Orthopaedics and Related Research*, *244*, 265–271.

Long, J. H., Adcock, B., & Root, R. G. (2002). Force transmission via axial tendons in undulating fish: a dynamic analysis. *Comparative Biochemistry and Physiology Part A: Molecular & Integrative Physiology*, *133*, 911–929.

Long, J., Hale, M., Mchenry, M., & Westneat, M. (1996). Functions of fish skin: flexural stiffness and steady swimming of longnose gar, Lepisosteus osseus. *Journal of*

Experimental Biology, *199*, 2139–2151.

Maganaris, C. N., Reeves, N. D., Rittweger, J., Sargeant, A. J., Jones, D. A., Gerrits, K., & De Haan, A. (2006). Adaptive response of human tendon to paralysis. *Muscle & Nerve*, *33*, 85–92.

Magnusson, S. P., & Kjaer, M. (2003). Region-specific differences in Achilles tendon cross-sectional area in runners and non-runners. *Journal of Applied Physiology*, *90*, 549–553.

Magnusson, S. P., & Kjaer, M. (2019). The impact of loading, unloading, ageing and injury on the human tendon. *The Journal of Physiology*, *597*, 1283–1298.

Marieb, E. N., & Hoehn, K. (2013). *Human Anatomy and Physiology* (Ninth). Pearson Education Inc.

Masson's Trichrome Staining Protocol for Collagen Fibers. (n.d.). Retrieved October 29, 2020, from http://www.ihcworld.com/_protocols/special_stains/masson_trichrome.htm

Nakashima, T., Hayashi, M., Fukunaga, T., Kurata, K., Oh-hora, M., Feng, J. Q., … Takayanagi, H. (2011). Evidence for osteocyte regulation of bone homeostasis through RANKL expression. *Nature Medicine*, *17*, 1231–1234.

Noble, B. S. (2008). The osteocyte lineage. *Archives of Biochemistry and Biophysics*, *473*, 106–111.

Nordvik, K., Kryvi, H., Totland, G. K., & Grotmol, S. (2005). The salmon vertebral body develops through mineralization of two preformed tissues that are encompassed by two layers of bone. *Journal of Anatomy*, *206*, 103–114.

Online Wed Fonts: Scalpel Free Icon. (n.d.). Retrieved October 16, 2018, from https://www.onlinewebfonts.com/icon/444904

Paten, J. A., Siadat, S. M., Susilo, M. E., Ismail, E. N., Stoner, J. L., Rothstein, J. P., & Ruberti, J. W. (2016). Flow-Induced Crystallization of Collagen: A Potentially Critical Mechanism in Early Tissue Formation. *American Chemical Society Nano*, *10*, 5027–5040.

Pereyra, M. E., Bona, P., Cerda, I. A., & Desántolo, B. (2019). Osteohistological correlates of muscular attachment in terrestrial and freshwater Testudines. *Journal of Anatomy*, *234*, 875–898.

Pilkey, W. D., Pilkey, D. F., & Bi, Z. (2020). Fundamentals of Stress Analysis. In *Peterson's Stress Concentration Factors* (pp. 1–87). Wiley.

Rigby, B. J., Hirai, N., Spikes, J. D., & Eyring, H. (1959). The Mechanical Properties of Rat Tail

Tendon The Journal of General Physiology. *The Journal of General Physiology*, *43*, 265–283.

Rønning, S. B., Østbye, T.-K., Krasnov, A., Vuong, T. T., Veiseth-Kent, E., Kolset, S. O., & Pedersen, M. E. (2017). The role of extracellular matrix components in pin bone attachments during storage—a comparison between farmed Atlantic salmon (Salmo salar) and cod (Gadus morhua L.). *Fish Physiology and Biochemistry*, *43*, 549–562.

Rossetti, L., Kuntz, L. A., Kunold, E., Schock, J., Müller, K. W., Grabmayr, H., … Bausch, A. R. (2017). The microstructure and micromechanics of the tendon–bone insertion. *Nature Materials*, *16*, 664–670.

Sai Chuen, F., Yau Chuk, C., Yim Ping, W., Wan Nar, W., Leung Kim, H., & Kai Ming, C. (2004). Immunohistochemical Characterization of Cells in Adult Human Patellar Tendons. *The Journal of Histochemistry & Cytochemistry*, *52*, 1151–1157.

Saino, H., Luther, F., Carter, D. H., Natali, A. J., Turner, D. L., Shahtaheri, S. M., & Aaron, J. E. (2003). Evidence for an extensive collagen Type III proximal domain in the rat femur II: Expansion with exercise. *Bone*, *32*, 660–668.

Sanchez, S., Dupret, V., Tafforeau, P., Trinajstic, K. M., Ryll, B., Gouttenoire, P.-J., … Ahlberg, P. E. (2013). 3D Microstructural Architecture of Muscle Attachments in Extant and Fossil Vertebrates Revealed by Synchrotron Microtomography. *PLOS ONE*, *8*, e56992.

Schwartz, A. G., Lipner, J. H., Pasteris, J. D., Genin, G. M., & Thomopoulos, S. (2013). Muscle loading is necessary for the formation of a functional tendon enthesis. *Bone*, *55*, 44–51.

Shadwick, R. E., Rapoport, H. S., & Fenger, J. M. (2002). Structure and function of tuna tail tendons. *Comparative Biochemistry and Physiology - A Molecular and Integrative Physiology*, *133*, 1109–1125.

Shah, R. R., Nerurkar, N. L., Wang, C. C., & Galloway, J. L. (2015). Tensile properties of craniofacial tendons in the mature and aged zebrafish. *Journal of Orthopaedic Research*, *33*, 867–873.

Short, E., & Johnson, R. B. (1990). Effects of Tooth Function on Adjacent Alveolar Bone and Sharpey's Fibers of the Rat Periodontiurn. *The Anatomical Record*, *227*, 391–396.

Subramanian, A., Kanzaki, L. F., Galloway, J. L., & Schilling, T. F. (2018). Mechanical force regulates tendon extracellular matrix organization and tenocyte morphogenesis through TGFbeta signaling. *ELife*, *7*, e38069.

Sugiyama, T., Price, J. S., & Lanyon, L. E. (2010). Functional adaptation to mechanical loading in both cortical and cancellous bone is controlled locally and is confined to the loaded bones. *Bone*, *46*, 314–321.

Summers, A. P., & Koob, T. J. (2002). The evolution of tendon--morphology and material properties. *Comparative Biochemistry and Physiology. Part A, Molecular & Integrative Physiology*, *133*, 1159–1170.

Summers, A. P., & Long, J. H. (2005). Skin and Bones, Sinew and Gristle: the Mechanical Behavior of Fish Skeletal Tissues. *Fish Physiology*, *23*, 141–177.

Suniaga, S., Rolvien, T., vom Scheidt, A., Fiedler, I. A. K., Bale, H. A., Huysseune, A., … Busse, B. (2018). Increased mechanical loading through controlled swimming exercise induces bone formation and mineralization in adult zebrafish. *Scientific Reports*, *8*, 3646.

Suzuki, D., Murakami, G., & Minoura, N. (2002). Histology of the bone-tendon interfaces of limb muscles in lizards. *Annals of Anatomy*, *184*, 363–377.

Suzuki, D., Murakami, G., & Minoura, N. (2003). Crocodilian bone-tendon and bone-ligament interfaces. *Annals of Anatomy*, *185*, 425–433.

Syme, D. A., & Shadwick, R. E. (2011). Red muscle function in stiff-bodied swimmers: there and almost back again. *Philosophical Transactions of the Royal Society B: Biological Sciences*, *366*, 1507–1515.

Thankam, F. G., Chandra, I. S., Kovilam, A. N., Diaz, C. G., Volberding, B. T., Dilisio, M. F., … Agrawal, D. K. (2018). Amplification of Mitochondrial Activity in the Healing Response Following Rotator Cuff Tendon Injury. *Scientific Reports*, *8*, 17027.

The Editors of Encyclopaedia Britannica. (2018). Periosteum. In *Britannica*. Encyclopaedia Britannica, Inc.

Thomopoulos, S., & Genin, G. M. (2013). The challenge of attaching dissimilar materials. In *Structural interfaces and attachments in biology* (pp. 3–17). Springer.

Thorpe, C. T., & Screen, H. R. C. (2016). Tendon Structure and Composition. In *Advances in Experimental Medicine and Biology* (pp. 3–10). Springer.

Torres, M., & Ramos, E. (2016). A New Method for Staining Ligaments and Tendons of Small Vertebrates. *Copeia*, *104*, 708–711.

Totland, G. K., Fjelldal, P. G., Kryvi, H., Løkka, G., Wargelius, A., Sagstad, A., … Grotmol, S. (2011). Sustained swimming increases the mineral content and osteocyte density of salmon

vertebral bone. *Journal of Anatomy*, *219*, 490–501.

Turcotte, C. M., Green, D. J., Kupczik, K., McFarlin, S., & Schulz-Kornas, E. (2020). Elevated activity levels do not influence extrinsic fiber attachment morphology on the surface of muscle-attachment sites. *Journal of Anatomy*, *236*, 827–839.

Turko, A. J., Kü Ltz, D., Fudge, D., Croll, R. P., Smith, F. M., Stoyek, M. R., & Wright, P. A. (2017). Skeletal stiffening in an amphibious fish out of water is a response to increased body weight. *Journal of Experimental Biology*, *220*, 361–3631.

Vader, D., Kabla, A., Weitz, D., & Mahadevan, L. (2009). Strain-Induced Alignment in Collagen Gels. *PLoS ONE*, *4*, e5902.

Van Der Meulen, M. C. H., Yang, X., Morgan, T. G., & Bostrom, M. P. G. (2009). The Effects of Loading on Cancellous Bone in the Rabbit. *Clinical Orthopaedics and Related Research*, *467*, 2000–2006.

Viidik, A., & Ekholm, R. (1968). Light and Electron Microscopic Studies of Collagen Fibers under Strain. *Zeitschrift Für Anatomie Und Entwicklungsgeschichte*, *127*, 154–164.

Voge, C. M., Kariolis, M., MacDonald, R. A., & Stegemann, J. P. (2008). Directional conductivity in SWNT-collagen-fibrin composite biomaterials through strain-induced matrix alignment. *Journal of Biomedical Materials Research Part A*, *86A*, 269–277.

Vogel, K. G., & Koob, T. J. (1989). Structural Specialization in Tendons under Compression. *International Review of Cytology*, *115*, 267–293.

Web Stock Review: Needle Clipart Medical. (n.d.). Retrieved November 2, 2020, from https://webstockreview.net/explore/needle-clipart-medical/

Westneat, M. W., Hoese, W., Pell, C. A., & Wainwright, S. A. (1993). The horizontal septum: Mechanisms of force transfer in locomotion of scombrid fishes (Scombridae, Perciformes). *Journal of Morphology*, *217*, 183–204.

Westneat, M. W., & Wainwright, S. A. (2001). 7. Mechanical design for swimming: muscle, tendon, and bone. *Fish Physiology*, *19*, 271–311.

Witten, P. E., & Huysseune, A. (2009). A comparative view on mechanisms and functions of skeletal remodelling in teleost fish, with special emphasis on osteoclasts and their function. *Biological Reviews*, *84*, 315–346.

Young, M. F. (2003). Bone matrix proteins: their function, regulation, and relationship to osteoporosis. *Osteoporosis International*, *14*, 35–42.

Zumwalt, A. (2006). The effect of endurance exercise on the morphology of muscle attachment sites. *Journal of Experimental Biology*, *209*, 444–454.

APPENDIX

Hematoxylin and Eosin Staining Protocol

Preparation of Staining Reagents

- Shandon™ Hematoxylin Stock Solution
  - Shandon™ Instant Hematoxylin
- Shandon™ Hematoxylin Working Solution
  - 1 part Hematoxylin stock solution and 1 part distilled water
- Eosin Stock Solution
  - 1.0 g of Eosin y; 20 mL of distilled water; 80 mL of 95% ethanol
- Eosin Working Solution
  - 1 part Eosin stock solution; 3 parts 80% ethanol
  - Add 0.5 mL of acetic acid/ 100 mL of working solution to intensify the stain
- Acid Alcohol
  - 1000 mL of 70% ethanol; 10 mL of hydrochloric acid
- Ammonia Water
  - 1000mL of tap water; 3 mL of 28% ammonium hydroxide

Staining Protocol

1. 3 changes of toluene, 5 minutes in each change
2. 3 changes of 100% ethanol, 7 dips in each change
3. Bring to distilled water for 5 minutes
4. Hematoxylin working solution for 18 minutes
5. Running tap water (rinse)
6. Acid alcohol, 2 dips
7. Running tap water (rinse)
8. Ammonia water for 1 minute
9. Running tap water for 8 minutes
10. 50% ethanol for 2 minutes
11. Eosin working solution for 35 seconds
12. 3 changes of 100% ethanol, 7 dips in each change
13. 3 changes of toluene, 7 dips in each change
14. Apply Permount™ and cover slip. Set slides out to dry.

Picrosirius Red Staining Protocol

Preparation of Staining Reagents

- 0.1% Picrosirius Red
    - 0.1 g of sirius red
    - 100 mL of aqueous 1.3% picric acid
- 0.01 N hydrochloric acid
    - Dilute from concentrated hydrochloric acid

Staining Protocol

1. 3 changes of toluene, 5 minutes in each change
2. 3 changes of 100% ethanol, 7 dips in each change
3. Distilled water for 5 minutes
4. Picrosirius Red for 1 hour
5. Wash in 0.01N hydrochloric acid (3 changes)
    a. 10 dips in first change
    b. 10 dips in second change
    c. 2 minutes in third change
6. 3 changes of 100% ethanol
7. 3 changes of toluene
8. Apply Permount™ and cover slip. Set slides out to dry.

Masson Trichrome Staining Protocol (modified from "Masson's Trichrome Staining Protocol for Collagen Fibers" [n.d.])

Staining Reagents

- Bouin's Solution
  - 150 mL of 1.3% picric acid
  - 50 mL of 4% paraformaldehyde
  - 10 mL of glacial acetic acid
- Weigert's Iron Hematoxylin
  - Stock Solution A:
    - 1 g of Weigert's Hematoxylin
    - 100 mL of 95% ethanol
  - Stock Solution B:
    - 4 mL of 29% ferric chloride in water (100 g ferric chloride/ 345 mL water)
    - 95 mL of distilled water
    - 1 mL of concentrated hydrochloric acid
- Aniline Blue Solution
  - 5 g of Aniline Blue
  - 4 mL of glacial acetic acid
  - 200 mL of distilled water
- Biebrich Scarlet-Acid Fuchsin Solution
  - 200 mL of distilled water
  - 2 mL of glacial acetic acid
  - 1.8 g of Scarlet Red
  - 0.2 g of Fuchsin
- 1:1 PMA/PTA Solution
  - 125 mL of 2.5% phosphotungstic acid (PTA)
  - 125 mL of 2.5% phosphomolybdic acid (PMA)

Staining Protocol

1. 3 changes of toluene, 5 minutes in each change
2. 3 changes of ethanol (95%, 70%, 50%), 7 dips in each change
3. Distilled water for 5 minutes
4. Bouin's solution for 1 hour at 56 °C
5. Rinse in running tap water for 8 minutes
6. Stain in Weigert's Iron Hematoxylin working solution for 10 minutes
7. Rinse in running warm tap water for 10 minutes
8. Wash in distilled water
9. Biebrich Scarlet-Acid Fuchsin solution for 15 minutes
10. Wash in distilled water
11. 2.5% PMA/2.5% PTA solution for 45 minutes
12. Aniline Blue solution for 9 minutes
13. Rinse briefly in distilled water
14. 1% acetic acid solution or 3.5 minutes
15. Wash in distilled water
16. 3 changes of ethanol (50%, 70%, 95%)

17. 3 changes of toluene, 7 dips in each change
18. Apply Permount™ and cover slip. Set slides out to dry.